Resource

Cell Reports

Distinct Transcriptional Responses across Tissue-Resident Macrophages to Short-Term and Long-Term Metabolic Challenge

Graphical Abstract

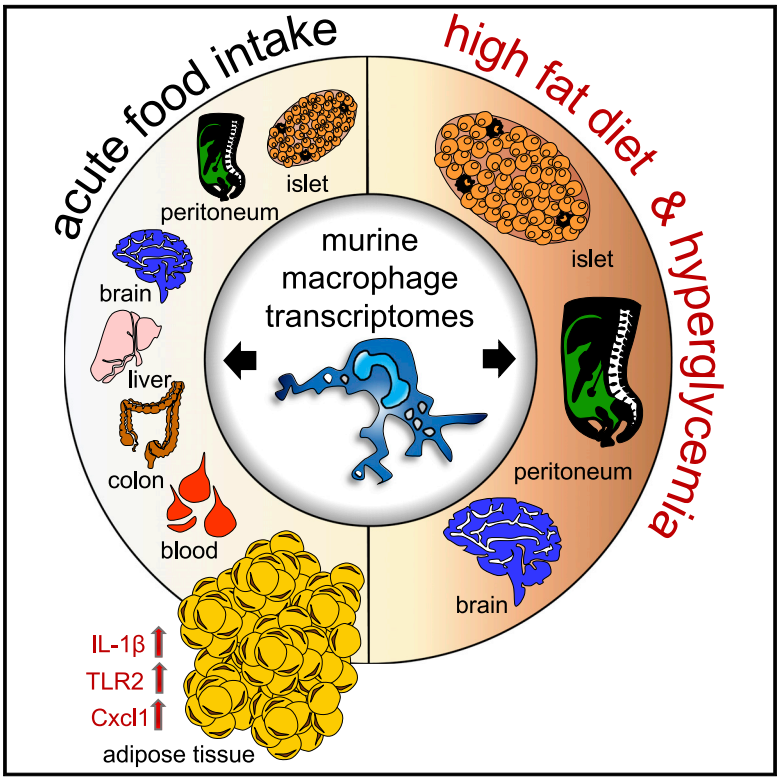

Authors

Urszula Brykczynska, Marco Geigges, Sophia J. Wiedemann, ..., Christoph Hess, Marc Y. Donath, Renato Paro

Correspondence

sophia.j.wiedemann@gmail.com

In Brief

Brykczynska et al. investigate the response of tissue-resident macrophages to short- and long-term nutritional challenges. They identify adipose tissue macrophages and the IL-1 pathway as early sensors of metabolic changes and propose a regulatory role for heat shock proteins in response to acute and chronic metabolic perturbances.

Highlights

- Transcriptome resource for scarce macrophage populations upon a single feeding
- Feeding upregulates the IL-1 pathway selectively in adipose tissue macrophages
- Heat shock proteins regulate macrophage responses to nutritional challenge

Brykczynska et al., 2020, Cell Reports *30*, 1627–1643
February 4, 2020
https://doi.org/10.1016/j.celrep.2020.01.005

CellPress

Cell Reports
Resource

Distinct Transcriptional Responses across Tissue-Resident Macrophages to Short-Term and Long-Term Metabolic Challenge

Urszula Brykczynska,[1,6] Marco Geigges,[1,6] Sophia J. Wiedemann,[2,6,8,*] Erez Dror,[2] Marianne Böni-Schnetzler,[2] Christoph Hess,[3,4,7] Marc Y. Donath,[2,6,7] and Renato Paro[1,5,6,7]
[1]Epigenomics Group, Department of Biosystems Science and Engineering, ETH Zürich, Basel, Switzerland
[2]Clinic of Endocrinology, Diabetes and Metabolism, University Hospital Basel and Department of Biomedicine, University of Basel, Basel, Switzerland
[3]Immunobiology Laboratory, Department of Biomedicine, University of Basel and University Hospital of Basel, Basel, Switzerland
[4]Department of Medicine, University of Cambridge, Cambridge, UK
[5]Faculty of Science, University of Basel, Basel, Switzerland
[6]These authors contributed equally
[7]Senior author
[8]Lead Contact
*Correspondence: sophia.j.wiedemann@gmail.com
https://doi.org/10.1016/j.celrep.2020.01.005

SUMMARY

The innate immune system safeguards the organism from both pathogenic and environmental stressors. Also, physiologic levels of nutrients affect organismal and intra-cellular metabolism and challenge the immune system. In the long term, over-nutrition leads to low-grade systemic inflammation. Here, we investigate tissue-resident components of the innate immune system (macrophages) and their response to short- and long-term nutritional challenges. We analyze the transcriptomes of six tissue-resident macrophage populations upon acute feeding and identify adipose tissue macrophages and the IL-1 pathway as early sensors of metabolic changes. Furthermore, by comparing functional responses between macrophage subtypes, we propose a regulatory, anti-inflammatory role of heat shock proteins of the HSP70 family in response to long- and short-term metabolic challenges. Our data provide a resource for assessing the impact of nutrition and over-nutrition on the spectrum of macrophages across tissues with a potential for identification of systemic responses.

INTRODUCTION

Increasing evidence shows that metabolic stress such as over-nutrition activates the immune system. Analogous to the action against pathogens, immune cells aim to restore homeostasis as a response to nutrient overdose (DiSpirito and Mathis, 2015). Simultaneously, over-nutrition alters the cellular metabolic repertoire. Activation and differentiation of immune cells are associated with various metabolic switches. Therefore, altered metabolism may also adversely affect immune cell functionality (O'Neill et al., 2016).

Gluco- and lipotoxicity driven by over-nutrition induce oxidative stress, inflammasome activation, and cytokine production by macrophages (DiSpirito and Mathis, 2015). Macrophages accumulate in large numbers in many different tissues of obese humans and mice (Ehses et al., 2007; Libby, 2012; Weisberg et al., 2003; Xu et al., 2003). In obese adipose tissue (Lumeng et al., 2007), these macrophages typically display an M1 phenotype and produce inflammatory cytokines such as TNF-α, IL-6, IL-1β, and IL-18, which drive insulin resistance. Furthermore, they contribute to multiple symptoms of the metabolic syndrome, such as islet failure and atherosclerosis (Donath, 2014; Moore et al., 2013).

Most attention has been given to adipose tissue macrophages (ATMs) in obesity. However, tissue-specific macrophages are found in most tissues. They support tissue homeostasis by clearing cellular debris and are essential for tissue immune surveillance by driving responses to infection and resolving inflammation (Davies and Taylor, 2015). Phenotypically and functionally, tissue-resident macrophages differ to a large extent. Indeed, the specific environment of a tissue influences the transcriptional programs of resident macrophages and shapes their functions according to the tissue's specific needs (Gautier et al., 2012; Gosselin et al., 2014; Lavin et al., 2014; Okabe and Medzhitov, 2014).

With high circulating levels of nutrients, all tissues become potentially affected by over-nutrition. The response of macrophages may, however, differ depending on their tissue-specific role and the level of exposure. Alternatively, a mutual and restricted response aiming to restore tissue homeostasis can be expected.

Among tissue-specific macrophages, microglia have recently attracted attention. In the mouse hypothalamus, microglia with an inflammatory gene expression profile accumulate as early as 3 days after initiation of high-fat diet (HFD) feeding (Baufeld et al., 2016). Furthermore, pro-inflammatory as well as anti-inflammatory responses occur in hypothalamic microglia during HFD (Baufeld et al., 2016; Gao et al., 2014; Valdearcos et al., 2014), suggesting that the response of microglia to over-nutrition is dynamic and temporally distinct.

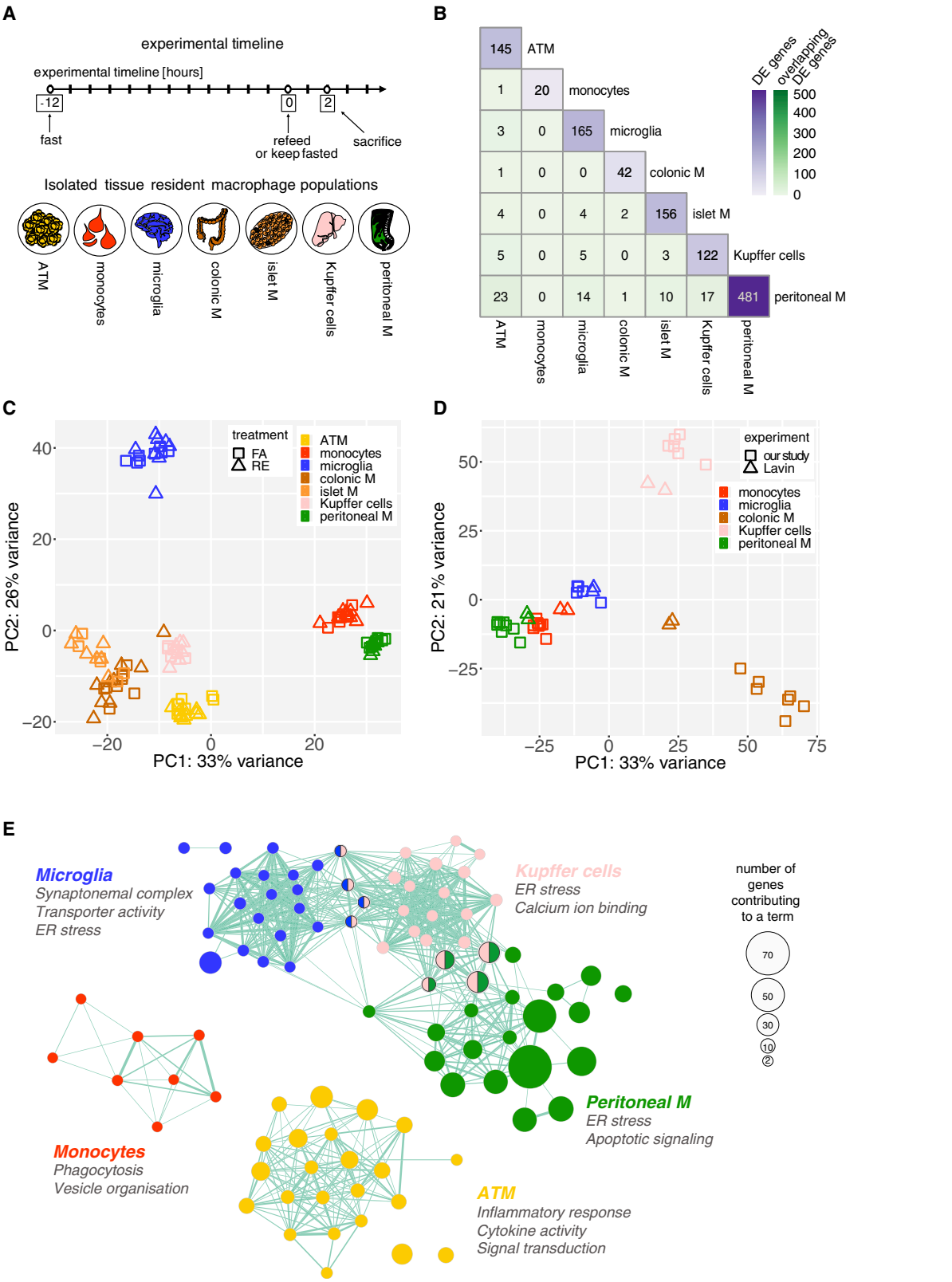

(legend on next page)

In pancreatic islets, macrophages are in close contact with β cells and have an important regulatory role in insulin production. Upon elevation of glucose levels, islet metabolic activity is increased, which induces reactive oxygen species (ROS) promoting the activation of NLRP3 inflammasome to enable IL-1β production (Maedler et al., 2002; Zhou et al., 2010). In addition, lipopolysaccharides (LPS) and free fatty acids activate TLR2 and TLR4, inducing NF-κB translocation and islet inflammation (Böni-Schnetzler et al., 2009; Pal et al., 2012). All these components induce low levels of islet-derived IL-1β, which in turn promotes IL-1-dependent cyto- and chemokines, including IL-6, IL-8, TNF-α, and MCP1. Furthermore, macrophages increase in number and activity (Butcher et al., 2014; Ehses et al.,2007; Richardson et al., 2009) and adopt a pro-inflammatory phenotype contributing to islet dysfunction and development of type 2 diabetes (Böni-Schnetzler and Meier, 2019).

Interestingly, food intake alone triggers a pro-inflammatory response in myeloid cells, leading to an increase of circulating IL-1β, which enhances insulin secretion (Dror et al., 2017). Therefore, there is a physiological role of myeloid cell-derived IL-1β that contrasts its deleterious role in driving insulin resistance and β cell failure in type 2 diabetes. Altogether this shows that macrophages are receptive to both short- and long-term nutritional signals and that different or even opposing effects can be expected (Baufeld et al., 2016; Dror et al., 2017).

To compare the effects of a selected regimen of nutritional conditions on immune cells, we sorted uniform macrophage populations for RNA sequencing (RNA-seq) analyses from different murine tissues. We provide a resource of transcriptomes from six tissue-resident macrophage populations and monocytes in response to feeding, as well as three tissue-resident macrophage populations after 8 weeks of HFD and a diabetic condition. We investigate how distinct or similar the macrophage response is across different tissues and how acute versus chronic nutritional stress affects their function. We identify a specific response of ATMs and the IL-1 pathway to food intake and propose an anti-inflammatory role of heat shock proteins (HSPs) across tissue-resident macrophages.

RESULTS

Distinctive Responses to Feeding across Tissue-Resident Macrophages

We first aimed to assess the transcriptional response to food intake across tissue-resident macrophages. Mice were fasted (FA) for 12 h (overnight) and then refed (RE) for 2 h with regular chow diet (Figure 1A). Tissue-resident macrophages from the adipose tissue (ATM), brain (microglia), colon, pancreatic islets, liver (Kupffer cells), and peritoneum and blood monocytes were collected using specific surface markers (Figure S1). Four hundred cells per cell type were isolated and used for RNA-seq. To account for scarcity of these cell types, we used RNA extraction, library preparation, and RNA-seq methods adapted from single-cell protocols (see STAR Methods). Six to ten biological replicates were analyzed per cell type. We detected 8,000 to 12,000 expressed genes per macrophage subtype (Figure S2A). Differential expression analysis was performed by comparing macrophages/monocytes from RE and FA mice in each tissue. Numbers of differentially expressed (DE) genes (adjusted p value [p_{adj}] < 0.05) varied among subtypes, with most changes in peritoneal macrophages (481 DE genes) (Figure 1B; Table S1), while monocytes were the least affected (20 DE genes). This did not depend on the significance threshold or analysis method used (Figures S2B and S2C). Because we aimed to distinguish common and divergent responses of macrophages in different tissues, we compared lists of DE genes. There was little overlap (0%–15% of common genes in all pairwise comparisons) between macrophage subtypes (Figure 1B) independent of the significance threshold and analysis method used (Figures S2B and S2C). This prompted us to assess the overall differences between gene expression in tissue-resident macrophages. Principal-component analysis (PCA) revealed more pronounced differences between macrophage subtypes than between the FA and RE conditions (Figure 1C). Diversity of transcriptomes of tissue-resident macrophages has previously also been reported (Gautier et al., 2012; Gosselin et al., 2014; Lavin et al., 2014; Okabe and Medzhitov, 2014). Therefore, we compared five macrophage subtypes analyzed by Lavin et al. (2014) with data from our study (FA samples). Macrophages from the same tissue from two studies were more similar than from different tissues in the same study (Figure 1D). Furthermore, hallmark tissue macrophage genes described by Lavin et al. (2014) had concordant expression profiles in our data (Figure S3A). These results confirm the high quality of our dataset, despite the small numbers of cells used and the distinct expression patterns of different tissue-resident macrophages found. In line with these observations, the response to feeding differs between macrophage populations and is lower in magnitude than the differences between the populations themselves.

ATMs Upregulate IL-1 Signaling upon Feeding

Next, we evaluated the response of macrophage subtypes at the functional level and performed Gene Ontology (GO) term analysis for up- and downregulated genes in the RE condition. Using

Figure 1. Feeding Affects the Transcriptomes of Tissue-Resident Macrophages

(A) Design of fasting and refeeding experiment.

(B) Numbers of differentially expressed (DE) genes between refed (RE) and fasted (FA) samples in each tissue-resident macrophage population (violet) and numbers of overlapping DE genes between macrophage subtypes (green) ($p < 0.05$). Color intensity of the background follows the number of DE genes.

(C) Principal-component analysis (PCA) of top 500 variable genes across all FA and RE samples of all tissue-resident macrophages.

(D) PCA of top 500 variable genes across FA samples in our study and samples from Lavin et al. (2014) in matching tissue-resident macrophages.

(E) Network of top significantly ($p_{adj} < 0.05$) over-represented GO terms among DE upregulated genes in RE versus FA comparison in tissue-resident macrophages. Color indicates macrophage subtype, node size indicates number of DE genes contributing to the term, and edges indicate overlapping DE genes contributing to the term. Representative terms are listed below each macrophage name.

See also Figures S1 and S2 and Tables S1 and S2.

Cytoscape and Enrichment Map software (Merico et al., 2010), we visualized the overlap of over-represented GO terms for five macrophage subtypes that showed significant terms (Figure 1E; Table S2). For upregulated genes in FA-RE, distinct sets of terms were over-represented for each subtype, with some overlapping terms in Kupffer cells, microglia, and peritoneal macrophages. ATMs showed multiple GO terms associated with inflammation, while no such GO terms were over-represented in any other subtype.

We confirmed this observation by analyzing genes involved in inflammation independent of the GO term gene sets (Figure 2A; Table S3). Clustering of fold changes (FCs) (RE versus FA) of these genes across macrophage subtypes revealed distinct upregulation of a pro-inflammatory gene cluster in ATMs that can be attributed to a local, low-grade inflammatory response in the adipose tissue. Differentially upregulated genes included the macrophage activation marker *Egr2* (Veremeyko et al., 2018), chemokines (*Cxcl1*, *Ccl2*, *Ccl7*, and *Ccl24*), and the cytokine *Il1b*. Importantly, IL-1β needs to be activated by the inflammasome and NLRP3, a crucial inflammasome component, was also present in this cluster. Of note, the absolute *Il1b* and *Nlrp3* expression levels were much higher in islet and colonic macrophages compared with other macrophages (Figure S3B), and expression of *Il1b* and *Nlrp3* did not increase upon feeding, indicating that these macrophages are in an activated state even without any stimulus (Ferris et al., 2017). In response to feeding, *Nlrp3* expression levels in ATMs reached the expression level in colonic macrophages (Figure S3B), pointing to a robust response. We validated the inflammatory response in ATMs using qPCR in two additional mouse cohorts. Both showed increased *Il1b*, *Cxcl1*, *Ccl3*, and *Tlr2* gene expression in response to feeding (Figure S4).

To assess which signaling pathways drive the activation of the IL-1 pathway, we performed pathway over-representation analysis of up- and downregulated genes in RE versus FA samples in ATMs using the KEGG (Kyoto Encyclopedia of Genes and Genomes; https://www.kegg.jp) and MSigDB (Molecular Signatures Database) canonical pathway databases (Subramanian et al., 2005; Figure 2B). The PI3K-AKT was the top upregulated pathway, along with receptor and effector genes such as *Tlr2*, *Itga9*, and *Mcl1*. The expression of genes of the AKT signaling cascade was not changed. However, this does not preclude pathway activation, as signaling events in this pathway may be mediated by phosphorylation. The JNK pathway is also implicated in *Il1b* activation. Interestingly, this pathway was suppressed in ATMs with the gene encoding for JNK (*Jun)* being downregulated in RE samples.

To further elucidate the transcriptional regulation of the pro-inflammatory response in ATMs upon feeding, we performed transcription factor (TF) binding motive enrichment analysis (Figures 2C and 2D). The consensus binding motive for RELA, a canonical member of the NF-κB family, was most significantly over-represented among upregulated genes in RE condition. Indeed, the canonical NF-κB pathway is responsible for transcriptional induction of pro-inflammatory genes including *Nrlp3* and *Il1b* upon stimulation (Liu et al., 2017). Furthermore, in the cluster of pro-inflammatory genes selectively activated in ATMs upon feeding (Figure 2A), we found two upregulated modulators of NF-κB activity, *Nfkbid* and *Nfkbiz*, and this was confirmed using qPCR (Figure S4). Collectively, these analyses suggest that AKT and NF-κB signaling may drive the IL-1 inflammatory activation in ATMs upon feeding.

Common and Differential Regulation of HSPs upon Feeding

GO term analysis for genes upregulated upon feeding revealed overlapping terms for Kupffer cells, microglia, and peritoneal macrophages, associated with endoplasmic reticulum (ER) stress and unfolded protein response (Figure 1E). HSP genes were the main DE genes contributing to these GO terms.

We further explored the differences in HSP expression and functionally associated genes (TFs, co-chaperones) across all macrophages (Figure 3A). Multiple genes from the HSP70 (*Hspa1a*, *Hspa1b*, *Hspa5*, *Hspa8*, and *Hsph1*), HSP90 (*Hsp90ab1* and *Hsp90b1*), and HSP40 (*Dnaja1* and *Dnajb2*) families were upregulated upon feeding in Kupffer cells, microglia, and peritoneal macrophages but not in islet, intestine, and ATMs and monocytes. Importantly, two genes encoding inducible HSP70 proteins (*Hspa1a* and *Hspa1b*) were significantly downregulated in RE versus FA samples in ATMs. Anti-inflammatory effects of the ER stress pathways and HSP70 proteins are known (Chung et al., 2008; Di Naso et al., 2015; Oh et al., 2012), and we hypothesize that ATMs downregulate HSP70 genes to activate physiological responses to feeding as described above. In peritoneal macrophages, we detected the largest number of upregulated HSP genes and the induction of TFs responsible for their expression: *Hsf1* and *Xbp1* (Figure 3A). Furthermore, TF-binding motive analysis in peritoneal macrophages (Figures 3B and 3C) revealed that the HSF1 motive is the top over-represented one among upregulated genes, suggesting that this TF might drive part of the changes observed upon feeding. HSF1 has been reported to inhibit *Il1b* expression by binding to the *Il1b* activating TF CEBPB (Xie et al., 2002). Accordingly, we have not observed any inflammatory response in peritoneal macrophages, while in ATMs that upregulate *Il1b*, HSF1 was the top predicted TF binding the downregulated genes (Figure 2D).

To validate the anti-inflammatory effect of HSP70 proteins, we activated peritoneal macrophages *in vitro* with LPS and adenosine triphosphate (ATP) to stimulate *Il1b* expression and IL-1β secretion (Figure 3D). To analyze the role of HSP70 proteins, we pre-treated the cells with a heat shock in the absence or in the presence of the HSPA1A agonist BGP-15 (O-[3-piperidino-2-hydroxy-1-propyl]-nicotinic amidoxime). The combination of these treatments indeed reduced IL-1β secretion (Figure 3D), and this was not due to reduced cellular viability (Figure S5). These data further support the anti-inflammatory effect of HSP70 proteins in macrophages.

Common Response to Food Intake across Macrophages

We observed little overlap between DE genes in different macrophage subtypes upon feeding (Figure 1A). We hypothesized that there may be genes with small changes that do not pass the significance threshold in all individual comparisons. To further investigate this potential common but mild response to food intake, we pooled all RE versus FA samples from all macrophage subtypes and treated them as biological replicates in the DE analysis

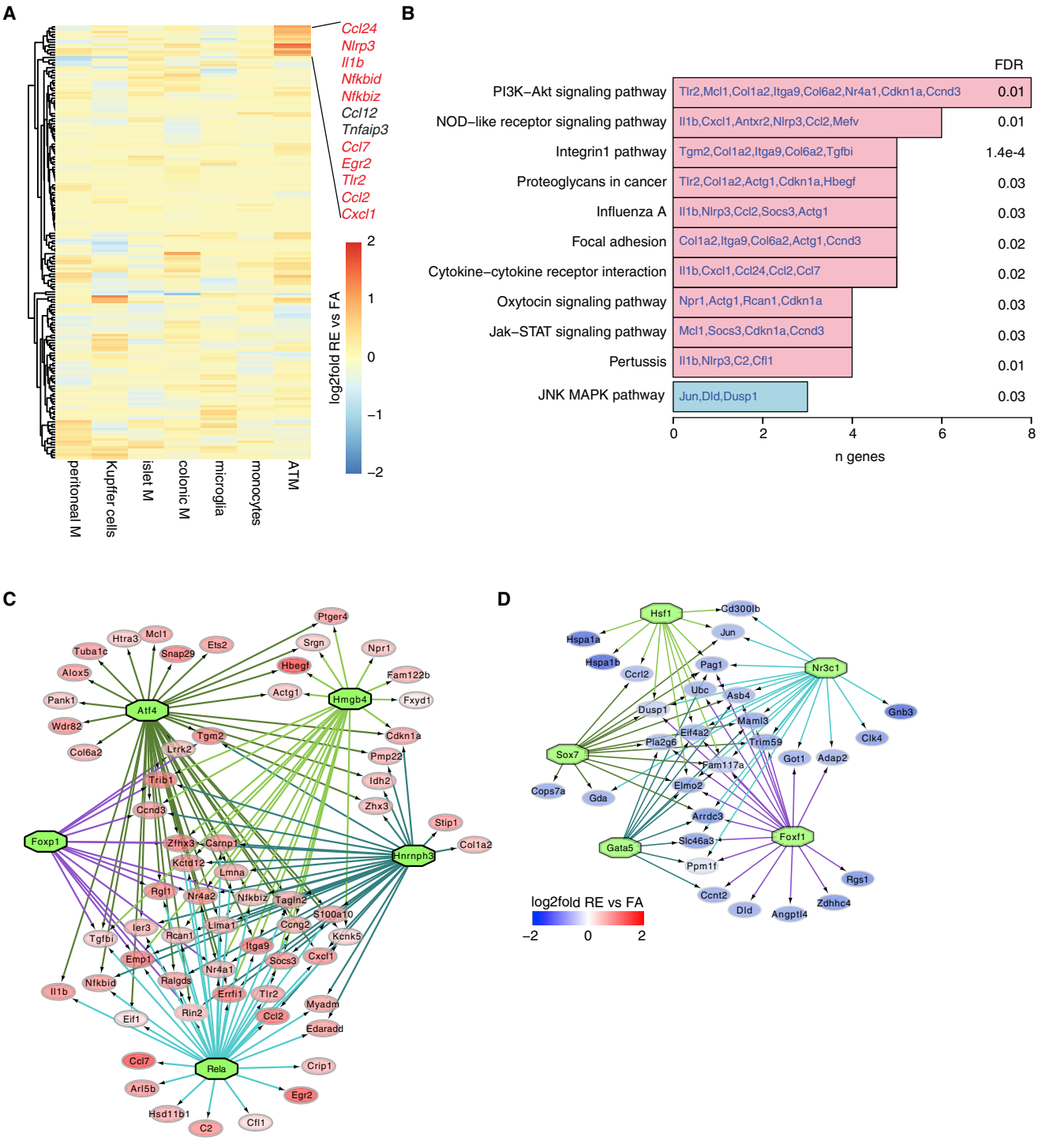

Figure 2. Adipose Tissue Macrophages Activate the IL-1 Pathway in Response to Feeding

(A) Heatmap of $\log_2$ fold changes (RE versus FA) of 170 selected inflammatory genes (provided in Table S3). The cluster of genes selectively activated in ATMs is highlighted and listed to the right of the heatmap. Red indicates genes that passed the significance threshold.

(B) Top significantly ($p_{adj} < 0.05$) over-represented pathways among upregulated (pink) and downregulated (blue) genes in ATMs in RE versus FA. DE genes contributing to the pathway are listed in each bar.

(C and D) Network of top five TFs with significantly over-represented binding motives among (C) upregulated or (D) downregulated genes upon RE in ATMs and their DE targets. Target node color indicates $\log_2$ fold change.

See also Figures S3 and S4 and Table S3.

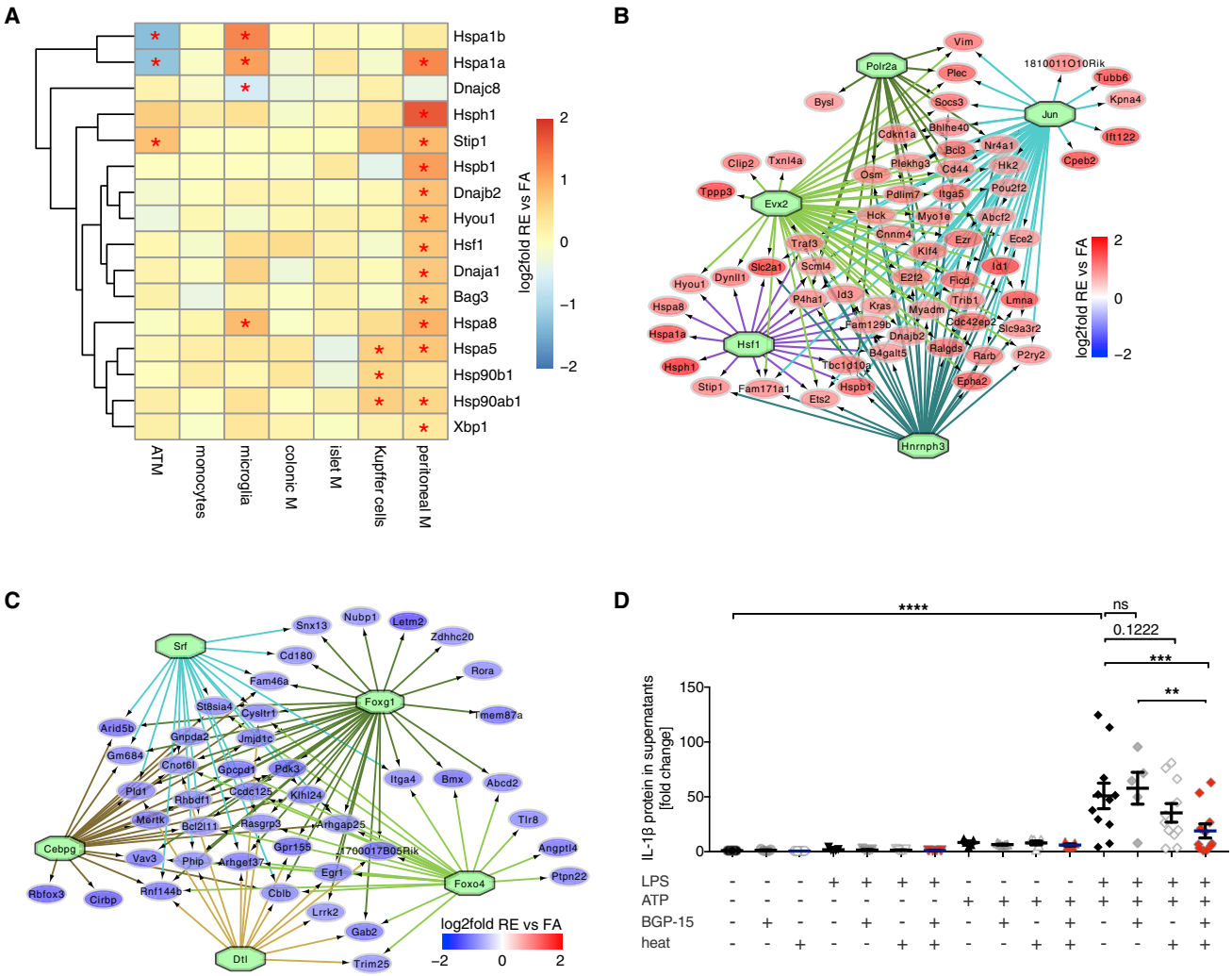

Figure 3. Heat Shock Proteins Are Differentially Regulated across Tissue-Resident Macrophages in Response to Feeding

(A) Heatmap of $\log_2$ fold changes (RE versus FA) of HSP genes that significantly change (red marks) in at least one macrophage subtype.

(B and C) Network of top five TFs with significantly over-represented binding motives among (B) upregulated or (C) downregulated genes upon RE in peritoneal macrophages and their DE targets. Target node color indicates $\log_2$ fold change. For visualization, the number of targets was restricted to (B) $\log_2$ fold change > 0.75 or (C) $\log_2$ fold change < −0.75.

(D) Activation of HSPA1A in peritoneal macrophages inhibits the release of IL-1β. Cells were subjected to either a heat shock condition (41°C), the HSPA1A activator BGP-15, or a combination thereof. IL-1β release was stimulated by LPS and ATP (biological replicates; n = 5–11).

Data are presented as arithmetic means of cell culture triplicates (single points) or arithmetic means of biological replicates (horizontal bars) ± SEM (error bars). Statistical analysis was performed using one-way ANOVA and the Holm-Sidak multiple-comparisons posttest. **p < 0.01, ***p < 0.001, and ****p < 0.0001. See also Figure S5.

(Figure 4A; Table S4). Among top upregulated genes, we found *Slc2a1* encoding for GLUT1, which is the main transporter in macrophage glucose metabolism and involved in the induction of inflammation (Freemerman et al., 2014). The individual $\log_2$ FC in macrophage subtypes varied between 0.03 and 1.46 and was highest in peritoneal macrophages (Figure 4B). This is consistent with IL-1β-dependent upregulation of GLUT1 and glucose uptake in macrophages *in vitro* as well as systemic upregulation of glucose uptake in response to feeding (Dror et al., 2017).

Interestingly, *Cpt1a*, a gene encoding a long chain fatty acid transporter acting at the rate-limiting step of fatty acid oxidation (FAO) was among the top downregulated genes in pooled RE versus FA samples (Figure 4A), with the largest downregulation in islet macrophages (Figure 4B). Differential up- and downregulation of *Slc2a1* and *Cpt1a* point to a change from fatty acid to glucose utilization. This metabolic switch has been described in multiple immune cell types upon activation (O'Neill et al., 2016), including macrophages upon HFD feeding (Freemerman et al., 2014; Malandrino et al., 2015).

We further performed pathway analysis for up- and downregulated genes from pooled RE versus FA comparison (Figure 4C; Table S5). Top upregulated pathways included "phagosome"

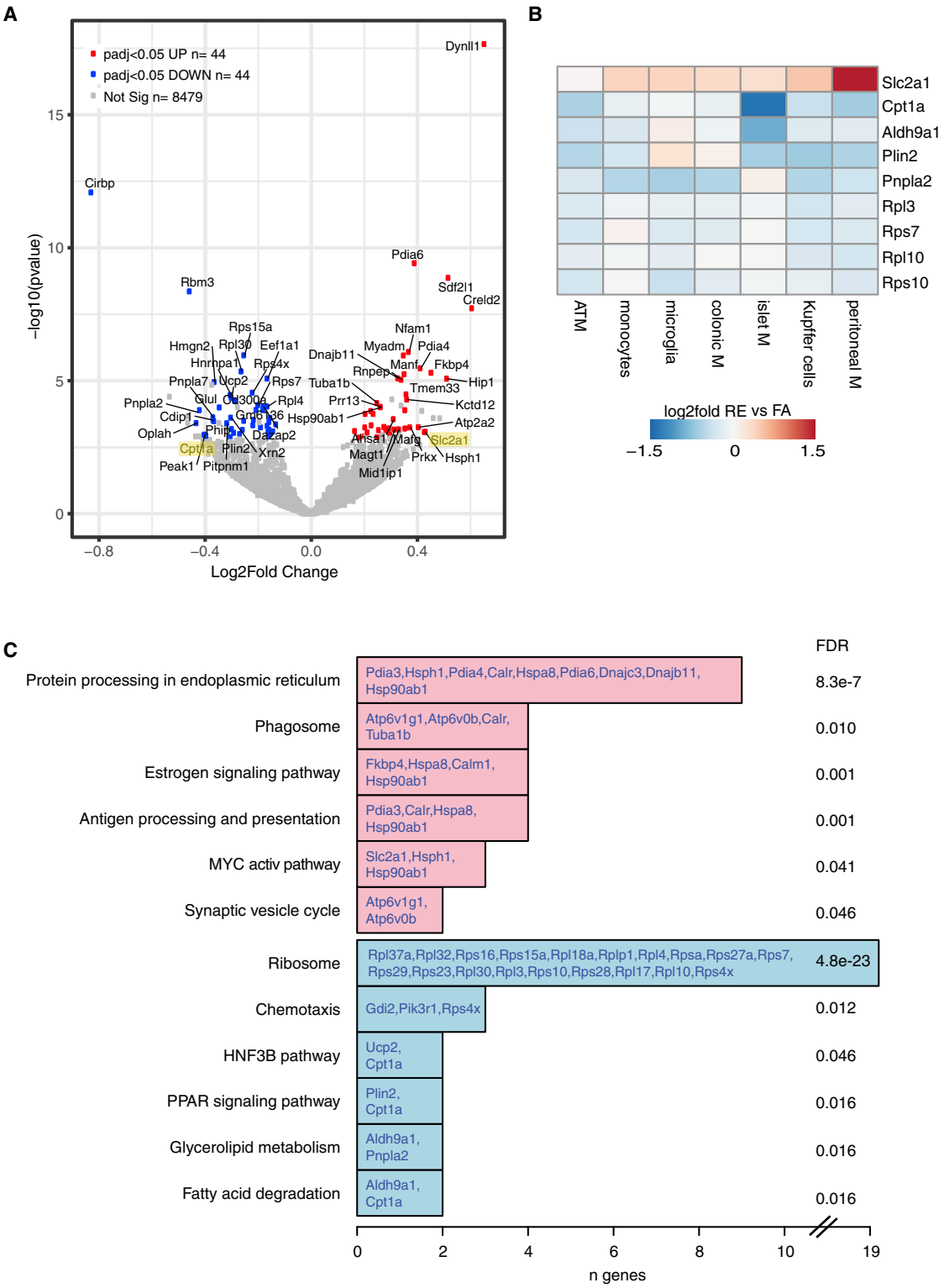

Figure 4. Common Metabolic Response to Feeding across Tissue-Resident Macrophages

(A) Volcano plot of DE analysis of all RE versus all FA samples from tissue-resident macrophages. DE genes with $p_{adj} < 0.05$ are marked in blue (downregulated) or red (upregulated). Gene names are displayed for top DE genes.

(legend continued on next page)

and "antigen processing and presentation," indicating activation of canonical macrophage functions. Top downregulated pathways comprised "glycerolipid metabolism" and "fatty acid oxidation," with contributing downregulated genes *Cpt1a*, *Aldh9a1*, *Plin2*, and *Pnpla2* (Figures 4B and 4C). This further supports the downregulation of fatty acid utilization and a systemic metabolic response to feeding across all tissue macrophages. Ribosomal small- and large-subunit genes were also downregulated across macrophage subtypes (Figures 4B and 4C), a previously described hallmark of macrophage activation (Varesio et al., 1992).

Altogether, this reveals that although a major part of the responses to feeding is divergent between the different tissue-resident macrophages, there remain common hallmarks of activation across all tissues.

Distinct Responses of Tissue-Resident Macrophages to HFD and Diabetic Conditions

Next we assessed the phenotype of selected tissue-resident macrophages to long-term metabolic challenge. Mice were fed an HFD for 4 weeks, then treated with a single low dose of streptozotocin (HFD-STZ) (130 mg/kg) or control to reduce β cell mass and to induce hyperglycemia (Figures S6A–S6C) and fed a HFD for another 4 weeks (Figure 5A). A third group consisted of initially weight-matched, chow food-fed littermates (ND). Islet macrophages, peritoneal macrophages, and microglia were isolated using fluorescence-activated cell sorting (FACS) (Figure S1) and subjected to RNA-seq.

Similar to the FA-RE experiment, the effect of HFD and HFD-STZ treatment was less prominent than the differences between macrophage subtypes (Figure 5B). However, PCA for samples from either islet or peritoneal macrophages, but not microglia, segregated the samples according to their treatment groups, ND, HFD, and HFD-STZ (Figure 5B).

HFD leads to elevated circulating lipid levels with toxic effects for tissues (DiSpirito and Mathis, 2015). The additional treatment of HFD-fed mice with STZ results in reduced plasma insulin and therefore diabetic blood glucose levels. Both conditions may trigger common and divergent responses in tissue-resident macrophages. Therefore, we first performed DE analysis in each macrophage subtype, comparing HFD and HFD-STZ samples with ND samples, followed by clustering of DE genes on the basis of their expression pattern across all conditions (Figures 5C–5F; Table S6), using the weighted correlation network analysis (WGCNA) (Zhang and Horvath, 2005). Furthermore, we compared the modules between the macrophage subtypes (Figure 5G) and annotated them with GO terms (Figure 5H; Table S7).

In islet macrophages, 1,348 DE genes were clustered into six modules (Figure 5D), with the largest numbers of genes in modules I-1 and I-5. In both modules, genes responded to both HFD and HFD-STZ conditions (up in module I-1 and down in module I-5), but the magnitude of the response was higher in the HFD-STZ condition. This indicates that the effect of lipids on the cells was enhanced by elevated blood glucose. Of note, module I-1 contained *Slc2a1* encoding glucose transporter GLUT1 and *Hk2*, a rate-limiting enzyme of glycolysis, again pointing to a metabolic switch to glucose utilization as described above. Arginase 2 encoded by *Arg2* was found in this module as well, while its isoform *Arg1* was downregulated in module I-5. *Arg1* expression is a hallmark of the anti-inflammatory M2 phenotype (Rath et al., 2014). In module I-1, we found *Il1rn*, which is an IL-1 receptor antagonist, indicating upregulation of anti-inflammatory mechanisms. Furthermore, module I-5 included several downregulated pro-inflammatory chemo- and cytokines. However, classical interferon-inducible genes such as *Ifi44*, *Oas1g*, and *Cd38* were upregulated. In module I-1, we further found upregulated *Igf1*, consistent with a recent report on islet macrophages secreting IGF1 that promotes islet regeneration (Nackiewicz et al., 2020). All DE genes with module annotation are listed in Table S6.

In peritoneal macrophages, 1,562 DE genes were clustered into seven modules (Figure 5E). The majority of upregulated genes were grouped into module P-4. They did not change upon HFD but were upregulated in the HFD-STZ condition. *Cpt1a*, which catalyzes the primary regulatory step of FAO, as well as the fatty acid transporter *Slc27a1*, were found in this cluster, together with the master transcriptional regulator of lipid metabolism *Pparg*. PPARγ coactivators *Ppaprgc1a* and *Ppargc1b*, found in module P-2, were also upregulated, in both HFD and HFD-STZ conditions. PPARγ activation and upregulation of FAO are hallmarks of metabolic reprogramming associated with anti-inflammatory responses (O'Neill et al., 2016). The majority of downregulated genes was part of modules P-5 and P-6, downregulated either in both HFD and HFD-STZ (P-5) or only in HFD-STZ (P-6). Consistent with a metabolic switch, we found *Hk1*, a rate-limiting enzyme of glycolysis, downregulated in module P-6. Altogether, these changes point to an anti-inflammatory metabolic phenotype of peritoneal macrophages in the HFD-STZ condition (see Table S6 for all DE genes with module annotation).

We systematically compared the responses in islet and peritoneal macrophages by checking their module overlaps (Figure 5G). We generally observed small numbers of overlapping genes. The largest and most significant overlap (24 genes) was between modules I-1 (genes up in HFD and HFD-STZ) in islet and P-4 in peritoneal macrophages (genes up in HFD-STZ). These included, among others, interferon-inducible genes described above and *Ms4a4a* and *Ms4a6d*. MS4A4A is a marker of alternatively activated M2 macrophages (Sanyal et al., 2017), and MS4A6D suppresses *Il1b* and *Nlrp3* expression in macrophages (Huang et al., 2019). Indeed, in both islet and peritoneal macrophages, we did not observe upregulation of *Il1b*, although it is an established hallmark of inflammation in ATMs in HFD-fed mice and obese humans (Bing, 2015; DiSpirito and Mathis, 2015).

(B) Heatmap of $\log_2$ fold changes from individual RE versus FA comparisons in each tissue macrophage subtype for selected genes involved in metabolic processes and of ribosomal subunits.

(C) Top significantly ($p_{adj} < 0.05$) over-represented pathways among upregulated (pink) and downregulated (blue) DE genes in all RE versus all FA samples from tissue-resident macrophages. DE genes contributing to the pathway are listed in each bar, and corresponding FDR values are listed on the right.

See also Tables S4 and S5.

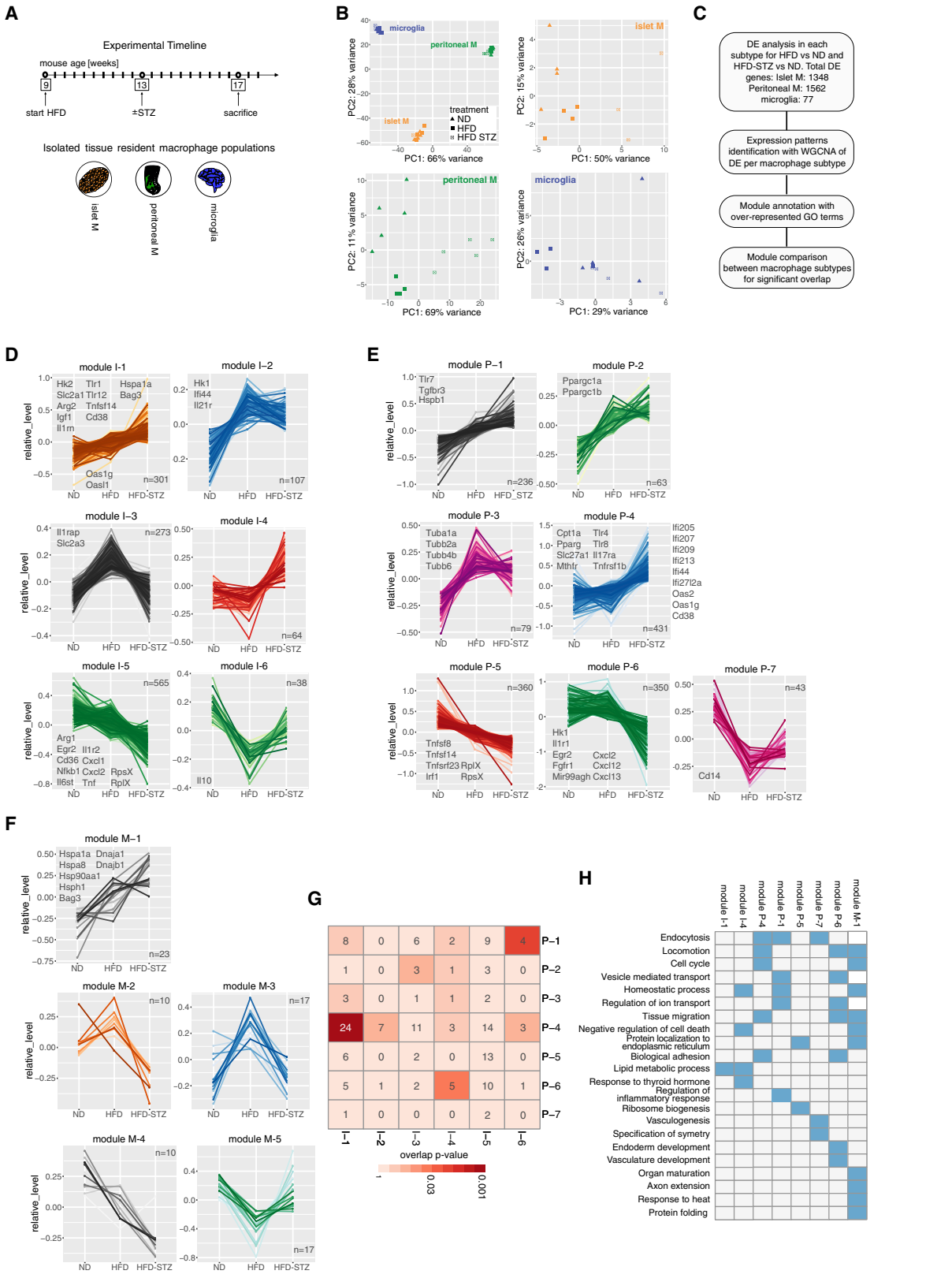

(legend on next page)

In microglia with only 77 DE genes, five modules were identified (Figure 5F). Module M-1 contained genes upregulated in both HFD and HFD-STZ conditions, with higher response in the latter, including multiple HSP genes: HSP40 family members *Dnaja1* and *Dnajb1*, HSP70 members *Hspa1a* and *Hspa8*, co-chaperones *Bag3* and *Hsph1*, and HSP90 family member *Hsp90aa1*. Interestingly, *Hspa1a* and *Hspa8* were not only upregulated in microglia upon long-term metabolic challenge but were also induced upon short-term feeding (Figure 3A). In hypothalamic microglia, an inflammatory response was observed after 3 days of HFD, which was attenuated after 8 weeks, with anti-inflammatory genes such as *Pparg* activated at that later time point (Baufeld et al., 2016). In our study with brain microglia analyzed after 8 weeks of HFD, we did not find any pro-inflammatory DE genes (Figure 5F; Table S6). Functional analysis revealed no inflammation-associated processes (Figure 5H; Table S7). These data further support an anti-inflammatory role of HSP70 gene upregulation.

As there were far fewer DE genes in microglia than in islet and peritoneal macrophages, we did not compare their modules. Of note, hormone or hormone-processing gene transcripts, which are abundantly expressed in endocrine β, α, and δ cells (*Ins2*, *Iapp*, *Gcg*, *Sst*, *Pcsk1*, and *Pcsk2*), were detected in islet macrophages but not in peritoneal macrophages and microglia (Figure S6D). This may result from engulfment of secretory vesicles (Ying et al., 2019) or phagocytosis of endocrine cells.

M1 Signature in Islet Macrophages and Fatty Acid Activation Signature in Peritoneal Macrophages

Activated macrophages are typically categorized into M1 IFNγ activated (pro-inflammatory) and M2 IL-4 activated (anti-inflammatory). To evaluate to what extend macrophage responses to HFD and STZ can be described by this simple categorization, we analyzed M1 and M2 signature gene (Jablonski et al., 2015) expression in our data (Figures 6A–6C). In this analysis, proper clustering of samples into experimental groups on the basis of signature genes indicated that these genes were DE between the analyzed conditions. For islet macrophages, hierarchical clustering of samples on the basis of 77 M1 signature genes resulted in perfect separation of ND and HFD and of ND and HFD-STZ experimental groups (Figure 6A). Furthermore, three genes of the M1 signature were significantly upregulated in HFD and seven in the HFD-STZ condition. Hierarchical clustering of samples on the basis of 45 M2 signature genes did not separate experimental groups for ND and HFD samples, whereas ND and HFD-STZ samples were perfectly separated. However, contributing genes were downregulated in HFD-STZ compared with ND samples, five of them significantly. Therefore, islet macrophages acquire an M1-like and suppress an M2 phenotype in response to HFD and STZ.

For peritoneal macrophages, hierarchical clustering of M1 signature genes nearly perfectly separated the groups (Figure 6B). However, genes contributing to the signature were both down- and upregulated. Clustering of samples on the basis of M2 signature perfectly separated the samples for ND and HFD-STZ groups, but again, both up- and downregulated genes contributed to it. In conclusion, peritoneal macrophages displayed a mix of M1-like and M2-like phenotypes, activating and suppressing both M1 and M2 phenotype elements.

In microglia, samples could not be separated into experimental groups with either M1 nor M2 signature (Figure 6C). None of the signature genes were DE, indicating that the response of microglia to HFD and STZ is not related to a classical type of activation.

The M1-M2 classification, although still commonly used, has been questioned (Martinez and Gordon, 2014; Murray et al., 2014). A larger spectrum of stimuli or *in vivo* rather than *in vitro* setups was used to extend this classification (Kratz et al., 2014; Xue et al., 2014). To characterize the phenotype of macrophages in HFD and STZ conditions, we used the spectrum model of macrophage activation proposed by Xue et al. (2014). They defined signatures of human macrophages subjected to 29 different *in vitro* stimuli and provided a framework for signature evaluation using gene set enrichment analysis (GSEA) (Subramanian et al., 2005). We used human homologs of mouse genes to query these signatures. For islet macrophages, the highest scoring (by enrichment score and p value) signature was the one derived from IFNγ for both HFD and HFD-STZ responses (Figure 6E), consistent with the good match with the above-described M1 signature of mouse macrophages. For peritoneal macrophages, the highest scoring signatures were those of linoleic acid and oleic acid in HFD and oleic acid in the HFD-STZ condition (Figure 6E). Therefore, a standard response to fatty acids, which is shared *in vitro* and *in vivo* and is distinct from classical M1 and M2 phenotypes, seems to exist in macrophages.

A Mixed M1/M2 Phenotype Is a Cellular Property of Peritoneal Macrophages

On the basis of size and F4/80 and CD11b expression, peritoneal cavity macrophages can be subdivided into two functionally

Figure 5. HFD and STZ Trigger Differential Responses in Islet and Peritoneal Macrophages and Microglia

(A) Design of HFD and HFD-STZ experiment.

(B) Principal-component analysis (PCA) of top 500 variable genes across ND, HFD, and HFD-STZ samples in all analyzed tissue-resident macrophages (top left) or in specific tissues: islet macrophages (orange, top right), peritoneal macrophages (green, bottom left), and microglia (blue, bottom right).

(C) Scheme of DE and clustering analysis for ND, HFD, and HFD-STZ samples.

(D–F) Modules of DE genes showing similar expression profile across ND, HFD, and HFD-STZ conditions in (D) islet macrophages, (E) peritoneal macrophages, and (F) microglia. Mean expression level of three to five biological replicates is displayed for each gene in three conditions. Number of genes belonging to each module and genes of special interest are indicated.

(G) Numbers of overlapping genes between modules from (D) (islet macrophages) and (E) (peritoneal macrophages). Color of the field indicates significance of the overlap (Fisher's exact test).

(H) Top over-represented GO terms for modules from (D)–(F). For a GO term that is significantly over-represented in a given module, the corresponding field is marked in blue. Modules that had no significant terms are not listed.

See also Figure S6 and Tables S6 and S7.

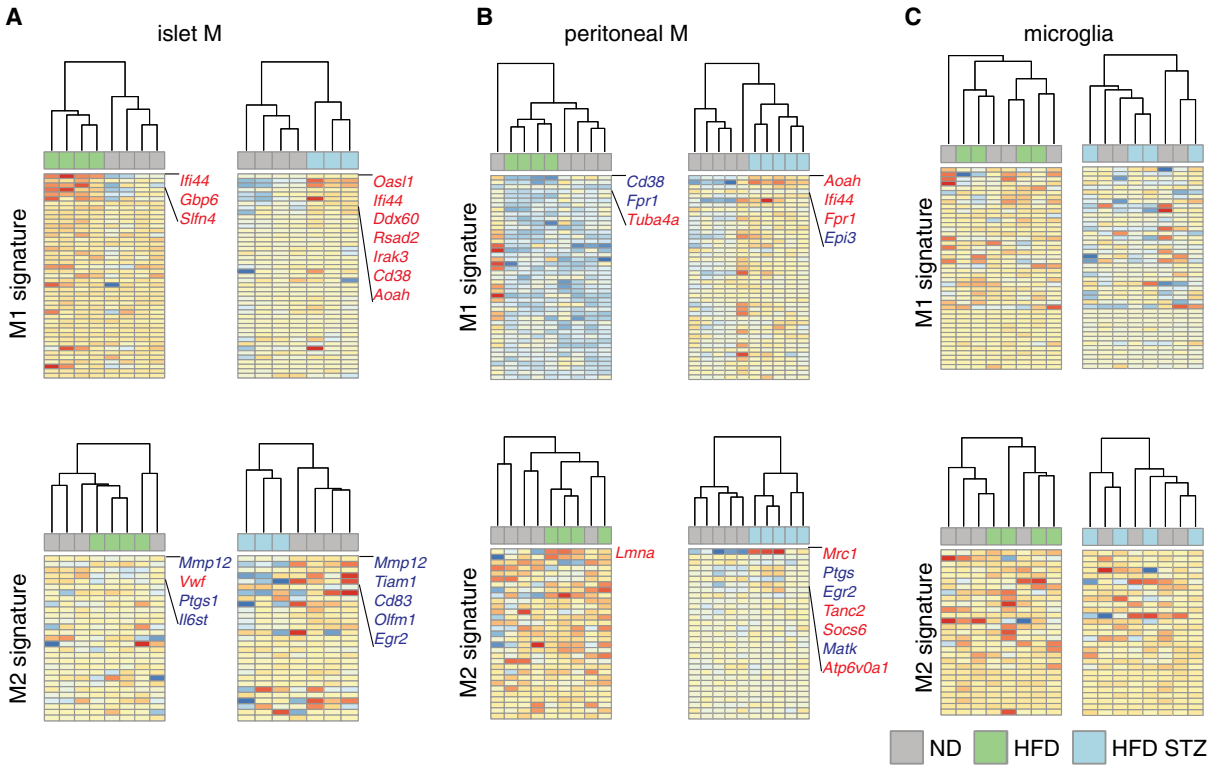

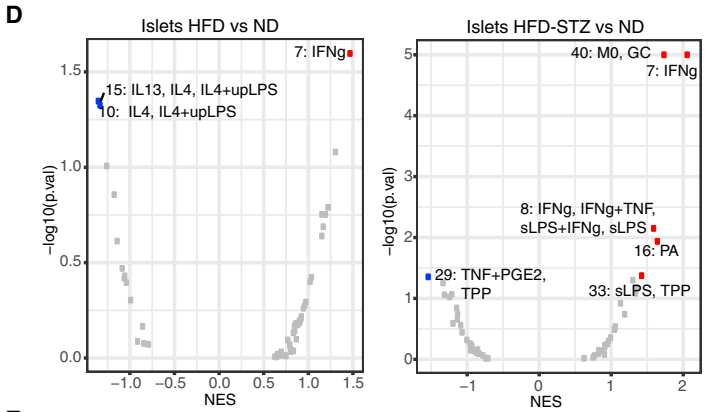

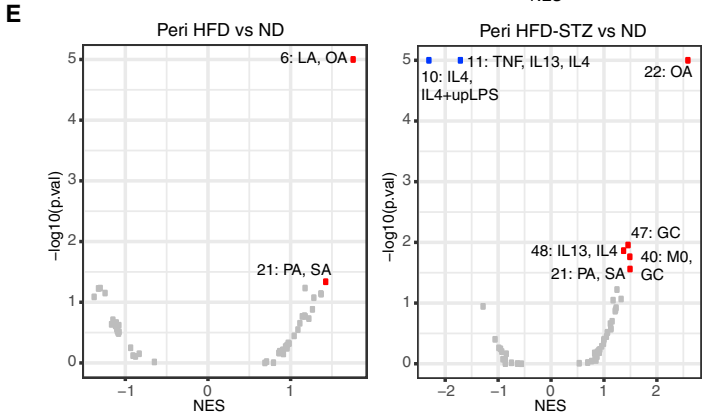

(legend on next page)

distinct subsets (Ghosn et al., 2010). To assess whether the mix of M1- and M2-like phenotypes observed in our RNA-seq dataset could be attributed to differences in these populations, protein levels of the M1-marker iNOS and the M2-marker CD206 were analyzed on small peritoneal macrophages (SPMs; defined as live single CD19− CD11c− F4/80^{low} CD11b^{low}) and large peritoneal macrophages (LPMs; defined as live single CD19− CD11c− F4/80^{high} CD11b^{high}) using flow cytometry (Figure S7). In agreement with previous studies (Ghosn et al., 2010), most peritoneal cavity macrophages were identified as LPMs, while SPMs only made up about 2%–5% of cells. LPMs in ND-fed mice were characterized by a mixed M1- and M2-like phenotype (Figure S7G). In contrast, the majority of SPMs were polarized toward an M1-like phenotype (Figure S7H). HFD did not change the proportions of LPMs and SPMs or their polarization profile compared with ND (Figures S7F–S7H), indicating that the mixed M1/M2 phenotype observed in our transcriptional analysis is not an artifact.

Short- versus Long-Term Metabolic Challenge

Macrophages protect tissues from pathogens but also maintain homeostasis upon physiological changes. Feeding results in temporarily elevated nutrients in the bloodstream and tissues. Long-term over-feeding provides constantly elevated nutrients in the circulation. This may potentially activate similar responses across tissue-resident macrophages. To evaluate this hypothesis, we compared the responses to feeding and to HFD in islet macrophages (Figure 7A), peritoneal macrophages (Figure 7B), and microglia (Figure 7C). We found very few overlapping genes between these two conditions. In islet macrophages, only seven genes were commonly DE, and just three of them changed in the same direction. *Cd36*, a fatty acid translocase, was downregulated in both conditions. As it is involved in NLRP3 inflammasome activation (Sheedy et al., 2013), its downregulation is consistent with lack of IL-1 pathway upregulation. As described above, the IL-1 pathway is constitutively active in islet macrophages, similarly to barrier macrophages (Ferris et al., 2017), and downregulation of *Cd36* may have a role in maintaining this steady state in response to both short- and long-term metabolic challenge.

In peritoneal macrophages (Figure 7B), we found 20 shared DE genes upregulated in HFD and feeding conditions. Interestingly, this common response included four tubulin (*Tubb6*, *Tuba1a*, *Tubb4b*, and *Tubb2a*), one laminin (*Lmna*), and one vimentin (*Vim*) gene, indicating cytoskeleton re-organization that could reflect phagocytosis, migration, and/or differentiation. Macrophages migrate from omentum to peritoneum (Okabe and Medzhitov, 2014), potentially also upon feeding, as macrophage numbers increased in peritoneum and decreased in omentum (Dror et al., 2017).

DISCUSSION

There is increasing evidence that metabolic syndromes such as obesity and diabetes affect the whole organism. The majority of research has focused on the adipose tissue as an obviously affected organ, and ATMs have been established as macrophages driving obesity-associated low-grade inflammation (Lumeng et al., 2007; Weisberg et al., 2003). Our study provides a resource to investigate the effect of over-nutrition and the physiological response to feeding across macrophages in additional tissues.

A large proportion of research in macrophages has been performed *in vitro*, providing a simplified view of macrophage responses, as the situation *in vivo* is more complex (Martinez and Gordon, 2014). However, populations of tissue-resident macrophages such as islet macrophages are sparse, and only advancements of technologies such as RNA-seq have enabled their analysis. In our study, we successfully isolated and analyzed transcriptomes of adipose tissue, colonic, islet, and peritoneal macrophages as well as Kupffer cells, microglia, and monocytes from purified populations as small as 400 cells. Still, there are several limitations of *in vivo* analyses. Macrophage populations in different tissues may be more heterogeneous than previously anticipated. For example, two macrophage subtypes were reported in islets: intra- and peri-islet macrophages (Ying et al., 2019). However, further identification of markers for specific subpopulations is needed. Another challenge of *in vivo* analysis is the necessity of different procedures to isolate macrophages in different tissues, and these may have an effect on the activation status of the cells. To overcome this issue, our comparisons between macrophages from different tissues are based on relative responses between treatment and control within one tissue, which cancels out isolation effects.

Our analysis of the spectrum of tissue-resident macrophages revealed that there is little overlap between the responses to short-term (Figures 1B and 1E) and long-term metabolic challenge (Figure 5G). This is consistent with highly variable transcriptomes of tissue-resident macrophages in the steady state (Gautier et al., 2012; Gosselin et al., 2014; Lavin et al., 2014; Okabe and Medzhitov, 2014). On the basis of our data, the response of each macrophage subtype could be further explored. Here, we focused on the low-grade inflammation of ATMs that we observed upon feeding (Figure 2). Our analyses

Figure 6. HFD and STZ Trigger M1-like Signature in Islet Macrophages and Fatty Acid Activation Signature in Peritoneal Macrophages

(A–C) Heatmaps of normalized expression values of ND, HFD, and HFD-STZ samples from (A) islet macrophages, (B) peritoneal macrophages, and (C) microglia of M1 and M2 signature genes (Jablonski et al., 2015). Genes are sorted on the basis of the adjusted p value in the current experiment, and genes with $p_{adj} < 0.05$ are highlighted and listed (red, upregulated genes; blue, downregulated genes). Clustering of biological replicates indicates genes that are changing in response to either HFD or HFD-STZ.

(D and E) Volcano plot of GSEA of genes responding to 29 stimuli reported by Xue et al. (2014) for DE genes from (D) islet macrophages and (E) peritoneal macrophages from HFD versus ND (left panel) and HFD-STZ versus ND (right panel) comparisons. Signatures significantly enriched among up- and downregulate genes ($p < 0.05$) are indicated in red and blue, respectively. Significant signatures are annotated with a number corresponding to numbering by Xue et al. (2014) and stimuli correlating with a given signature are listed.

See also Figure S7.

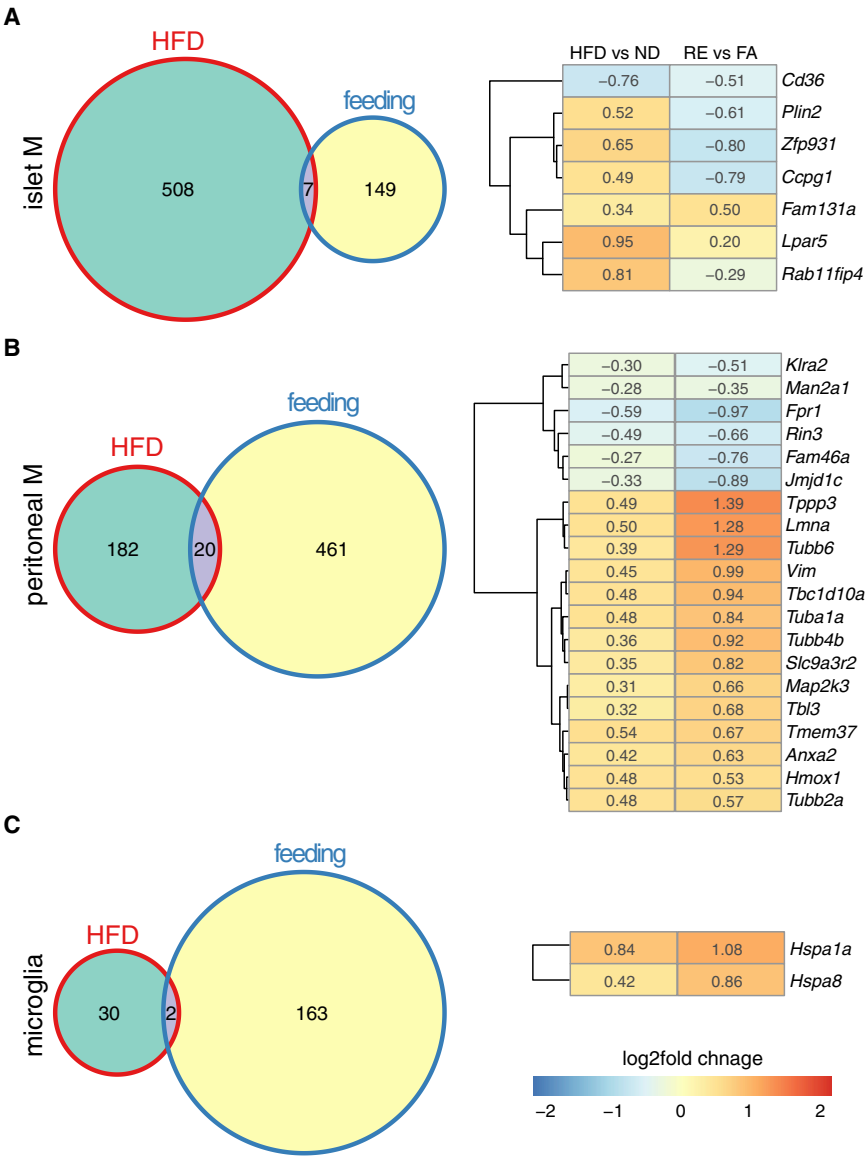

Figure 7. Response to Short- versus Long-Term Metabolic Challenge Is Different in Tissue-Resident Macrophages

Venn diagram of the numbers of DE genes from HFD versus ND and RE versus FA comparisons and heatmap of $\log_2$ fold changes of overlapping genes (from the Venn diagram intersection) in (A) islet macrophages, (B) peritoneal macrophages, and (C) microglia.

with RNA-seq and qPCR revealed an early first response to feeding characterized by the activation of the pro-inflammatory IL-1 pathway (Figure 2A; Figure S4), potentially driven by AKT and NF-κB signaling (Figures 2B and 2C). In line with this observation, physiological activation of pro-inflammatory pathways is required for mouse adipose tissue expansion and remodeling (Wernstedt Asterholm et al., 2014). Furthermore, human pre-adipocytes and adipocytes express the IL-1 receptor 1 (*Il1r1*), and IL-1β regulates metabolic genes (Caër et al., 2017). Together, these findings point to a role of ATMs and the IL-1 system in the regulation of adipose tissue biology upon feeding. Furthermore, an increase of IL-1β in the circulation has been observed in mice 2 h after feeding. This led to enhanced insulin secretion and glucose uptake into peritoneal macrophages via GLUT1 transporter (Dror et al., 2017). Consistently, we observed systemic upregulation of *Slc2a1* across tissue-resident macrophages (Figures 4A and 4B) and propose that ATMs might be a major source of the increased IL-1β upon feeding.

As described before (Calderon et al., 2015; Ferris et al., 2017), we observed much higher absolute levels of *Il1b* and *Nlrp3* in colonic and islet macrophages, pointing to constitutively active IL-1 signaling (Figure S3B). This may explain why the expression of these genes is not increased upon feeding or the HFD or HFD-STZ condition. Nevertheless, islet macrophages of HFD- and HFD-STZ-treated mice can be classified as M1 (Figure 6A) and IFNγ activated (Figure 6D). This suggests that the steady-state pro-inflammatory phenotype is enhanced under these conditions, consistent with islet inflammation in response to elevated glucose and lipids (Böni-Schnetzler et al., 2008, 2009; Ying et al., 2019).

In ATMs, a distinct phenotype associated with obesity and diabetes, termed metabolic activation, has been described (Kratz et al., 2014). It contains elements of both classical M1 (pro-inflammatory) and alternative M2 (anti-inflammatory) activation hallmarks. Here, we described that a mix of M1 and M2 signatures can be similarly detected in peritoneal macrophages (Figure 6B). Furthermore, they were classified as lipid activated (Figure 6E) and upregulated *Pparg* and lipid metabolism genes (Figure 5E), similarly as described for metabolic activation in ATMs (Kratz et al., 2014).

Across analyzed macrophages subtypes and treatments, we observed upregulation of HSP genes, mainly from the HSP70/HSP90 chaperone system (HDSP40, HSP70, and HSP90 families) (Figures 3A and 5D–5F), which is further supported by upregulation of HSP driving TFs (*Hsf1* and *Xbp1*) and TF enrichment motive analysis in peritoneal macrophages (Figure 3B). Downregulation of the two HSP70 family members *Hspa1a* and *Hspa1b* is observed only in ATMs upon feeding (Figure 3A). This was the only condition for which we observed upregulation of the IL-1 pathway (Figure 2A). The anti-correlation between HSP expression and IL-1 pathway activity is also supported by HSF1's function in repressing *Il1b* (Xie et al., 2002). Hence, we propose an anti-inflammatory role of HSP70 members in

tissue-resident macrophages upon metabolic challenge. The main functions of the HSP70/HSP90 chaperone system are the assistance of proper protein folding in the ER and degradation of misfolded or aggregated proteins (Schopf et al., 2017). HSPs are also involved in immunity, inflammation, and neurodegeneration (Lackie et al., 2017; Lee and Repasky, 2012). Anti-inflammatory properties of the HSP70 family and specifically of HSPA1A have been described, and the HSPA1A agonist molecule BGP-15 had positive effects in trials against diabetes and adverse effects of obesity (Chung et al., 2008; Henstridge et al., 2014; Literáti-Nagy et al., 2012). We used this molecule in a validation experiment and confirmed the anti-inflammatory effect of this HSPA1A agonist on macrophages, as measured by decrease of IL-1β secretion (Figure 3D). Mechanistically, downregulation of *Il1b* expression could be further explained by inhibitory effects of HSP70 on the NF-κB pathway. HSP70 was shown to destabilize TAK1, an activator of NF-κB pathway, through competition for HSP90 binding (Cao et al., 2012) and to destabilize the TAK1 interactor TRAF6 (Chen et al., 2006).

In contrast to previously reported anti- or pro-inflammatory responses (Baufeld et al., 2016; Gao et al., 2014; Valdearcos et al., 2014), we saw few changes in HFD and HFD-STZ conditions in microglia (Figure 5F). As the response changes in the course of HFD, we may have missed it at the 8 week time point. Furthermore, the magnitude of the reported changes in inflammatory gene expression does not exceed 1.5-fold. In fact, all previous studies focused on hypothalamic microglia (Baufeld et al., 2016; Gao et al., 2014; Valdearcos et al., 2014). Therefore, the HFD-induced effect may have been masked in our whole-brain microglia analysis. Importantly, in the fasting-refeeding experiment, we observed similar numbers of DE genes in microglia (Figure 1B) as in other macrophages subtypes indicating that we did not face a technical issue with microglia cells.

In summary, we provide a resource that will help dissect the role of tissue-resident macrophages in response to nutrition in both physiological and chronically overdosed conditions. We pinpoint ATMs and the IL-1 pathway as early sensors of nutritional status, an observation that awaits further evaluation and exploration.

STAR★METHODS

Detailed methods are provided in the online version of this paper and include the following:

- KEY RESOURCES TABLE
- LEAD CONTACT AND MATERIALS AVAILABILITY
- EXPERIMENTAL MODEL AND SUBJECT DETAILS
- METHOD DETAILS
  - Animal husbandry
  - Primary cell isolation
  - Cell culture
  - Flow cytometry
  - RNA extraction for validation and qPCR
  - Assays for protein measurements
  - RNA extraction for RNA-Seq
  - Sample preparation and RNA sequencing
  - Processing of RNA-Seq data
- QUANTIFICATION AND STATISTICAL ANALYSIS
  - General Information
  - Differential expression analysis
  - Principal component analysis (PCA)
  - Gene set and TF motive enrichment
  - Clustering of genes with correlated expression pattern
  - Signature enrichment analysis
  - Analyses of functional and validation studies
- DATA AND CODE AVAILABILITY

SUPPLEMENTAL INFORMATION

Supplemental Information can be found online at https://doi.org/10.1016/j.celrep.2020.01.005.

ACKNOWLEDGMENTS

Work of U.B., M.G., and R.P. was supported by ETH Zurich. M.G. is a member of the Life Science Zurich Graduate School and supported by a fellowship from the German Academic Scholarship Foundation. This study was supported by the Swiss National Science Foundation, Margot und Erich Goldschmidt & Peter René Jacobson-Stiftung (to S.J.W.), and the alumni of the medical faculty of the University of Basel (to S.J.W.). We thank D. Labes, E. Traunecker, and L. Raeli, FACS facility of the Department of Biomedicine of the University of Basel for help with cell sorting and K. Eschbach and C. Beisel, Genomics Facility Basel, for assistance with RNA-seq. We thank M. Okoniewski, ETH Scientific IT Services (SIS), for help with data analysis and critical reading of the manuscript.

AUTHOR CONTRIBUTIONS

M.Y.D., M.B.-S., C.H., R.P., U.B., M.G., and S.J.W. designed the experiments. S.J.W., E.D., and M.G. performed the experiments. U.B. analyzed the RNA-seq data. U.B., M.G., and S.J.W. wrote the manuscript with input from M.Y.D., M.B.-S., C.H., and R.P.

DECLARATION OF INTERESTS

The authors declare no competing interests.

Received: July 4, 2019
Revised: November 6, 2019
Accepted: December 31, 2019
Published: February 4, 2020

REFERENCES

Alhamdoosh, M., Law, C.W., Tian, L., Sheridan, J.M., Ng, M., and Ritchie, M.E. (2017). Easy and efficient ensemble gene set testing with EGSEA. F1000Res. *6*, 2010.

Baufeld, C., Osterloh, A., Prokop, S., Miller, K.R., and Heppner, F.L. (2016). High-fat diet-induced brain region-specific phenotypic spectrum of CNS resident microglia. Acta Neuropathol. *132*, 361–375.

Benjamini, Y., and Hochberg, Y. (1995). Controlling the false discovery rate: a practical and powerful approach to multiple testing. J. Roy. Stat. Soc. Ser. B. *57*, 289–300.

Bing, C. (2015). Is interleukin-1β a culprit in macrophage-adipocyte crosstalk in obesity? Adipocyte *4*, 149–152.

Bolger, A.M., Lohse, M., and Usadel, B. (2014). Trimmomatic: a flexible trimmer for Illumina sequence data. Bioinformatics *30*, 2114–2120.

Böni-Schnetzler, M., and Meier, D.T. (2019). Islet inflammation in type 2 diabetes. Semin. Immunopathol. *41*, 501–513.

Böni-Schnetzler, M., Thorne, J., Parnaud, G., Marselli, L., Ehses, J.A., Kerr-Conte, J., Pattou, F., Halban, P.A., Weir, G.C., and Donath, M.Y. (2008). Increased interleukin (IL)-1beta messenger ribonucleic acid expression in beta -cells of individuals with type 2 diabetes and regulation of IL-1beta in human islets by glucose and autostimulation. J. Clin. Endocrinol. Metab. *93*, 4065–4074.

Böni-Schnetzler, M., Boller, S., Debray, S., Bouzakri, K., Meier, D.T., Prazak, R., Kerr-Conte, J., Pattou, F., Ehses, J.A., Schuit, F.C., and Donath, M.Y. (2009). Free fatty acids induce a proinflammatory response in islets via the abundantly expressed interleukin-1 receptor I. Endocrinology *150*, 5218–5229.

Butcher, M.J., Hallinger, D., Garcia, E., Machida, Y., Chakrabarti, S., Nadler, J., Galkina, E.V., and Imai, Y. (2014). Association of proinflammatory cytokines and islet resident leucocytes with islet dysfunction in type 2 diabetes. Diabetologia *57*, 491–501.

Caër, C., Rouault, C., Le Roy, T., Poitou, C., Aron-Wisnewsky, J., Torcivia, A., Bichet, J.C., Clément, K., Guerre-Millo, M., and André, S. (2017). Immune cell-derived cytokines contribute to obesity-related inflammation, fibrogenesis and metabolic deregulation in human adipose tissue. Sci. Rep. *7*, 3000.

Calderon, B., Carrero, J.A., Ferris, S.T., Sojka, D.K., Moore, L., Epelman, S., Murphy, K.M., Yokoyama, W.M., Randolph, G.J., and Unanue, E.R. (2015). The pancreas anatomy conditions the origin and properties of resident macrophages. J. Exp. Med. *212*, 1497–1512.

Cao, X., Yue, L., Song, J., Wu, Q., Li, N., Luo, L., Lan, L., and Yin, Z. (2012). Inducible HSP70 antagonizes IL-1β cytocidal effects through inhibiting NF-kB activation via destabilizing TAK1 in HeLa cells. PLoS ONE *7*, e50059.

Chen, H., Wu, Y., Zhang, Y., Jin, L., Luo, L., Xue, B., Lu, C., Zhang, X., and Yin, Z. (2006). Hsp70 inhibits lipopolysaccharide-induced NF-kappaB activation by interacting with TRAF6 and inhibiting its ubiquitination. FEBS Lett. *580*, 3145–3152.

Chung, J., Nguyen, A.K., Henstridge, D.C., Holmes, A.G., Chan, M.H., Mesa, J.L., Lancaster, G.I., Southgate, R.J., Bruce, C.R., Duffy, S.J., et al. (2008). HSP72 protects against obesity-induced insulin resistance. Proc. Natl. Acad. Sci. USA *105*, 1739–1744.

Dalmas, E., Lehmann, F.M., Dror, E., Wueest, S., Thienel, C., Borsigova, M., Stawiski, M., Traunecker, E., Lucchini, F.C., Dapito, D.H., et al. (2017). Interleukin-33-Activated Islet-Resident Innate Lymphoid Cells Promote Insulin Secretion through Myeloid Cell Retinoic Acid Production. Immunity *47*, 928–942.

Davies, L.C., and Taylor, P.R. (2015). Tissue-resident macrophages: then and now. Immunology *144*, 541–548.

Di Naso, F.C., Porto, R.R., Fillmann, H.S., Maggioni, L., Padoin, A.V., Ramos, R.J., Mottin, C.C., Bittencourt, A., Marroni, N.A., and de Bittencourt, P.I., Jr. (2015). Obesity depresses the anti-inflammatory HSP70 pathway, contributing to NAFLD progression. Obesity (Silver Spring) *23*, 120–129.

DiSpirito, J.R., and Mathis, D. (2015). Immunological contributions to adipose tissue homeostasis. Semin. Immunol. *27*, 315–321.

Dobin, A., Davis, C.A., Schlesinger, F., Drenkow, J., Zaleski, C., Jha, S., Batut, P., Chaisson, M., and Gingeras, T.R. (2013). STAR: ultrafast universal RNA-seq aligner. Bioinformatics *29*, 15–21.

Donath, M.Y. (2014). Targeting inflammation in the treatment of type 2 diabetes: time to start. Nat. Rev. Drug Discov. *13*, 465–476.

Dror, E., Dalmas, E., Meier, D.T., Wueest, S., Thévenet, J., Thienel, C., Timper, K., Nordmann, T.M., Traub, S., Schulze, F., et al. (2017). Postprandial macrophage-derived IL-1β stimulates insulin, and both synergistically promote glucose disposal and inflammation. Nat. Immunol. *18*, 283–292.

Durinck, S., Spellman, P.T., Birney, E., and Huber, W. (2009). Mapping identifiers for the integration of genomic datasets with the R/Bioconductor package biomaRt. Nat. Protoc. *4*, 1184–1191.

Ehses, J.A., Perren, A., Eppler, E., Ribaux, P., Pospisilik, J.A., Maor-Cahn, R., Gueripel, X., Ellingsgaard, H., Schneider, M.K., Biollaz, G., et al. (2007). Increased number of islet-associated macrophages in type 2 diabetes. Diabetes *56*, 2356–2370.

Ferris, S.T., Zakharov, P.N., Wan, X., Calderon, B., Artyomov, M.N., Unanue, E.R., and Carrero, J.A. (2017). The islet-resident macrophage is in an inflammatory state and senses microbial products in blood. J. Exp. Med. *214*, 2369–2385.

Freemerman, A.J., Johnson, A.R., Sacks, G.N., Milner, J.J., Kirk, E.L., Troester, M.A., Macintyre, A.N., Goraksha-Hicks, P., Rathmell, J.C., and Makowski, L. (2014). Metabolic reprogramming of macrophages: glucose transporter 1 (GLUT1)-mediated glucose metabolism drives a proinflammatory phenotype. J. Biol. Chem. *289*, 7884–7896.

Gao, Y., Ottaway, N., Schriever, S.C., Legutko, B., García-Cáceres, C., de la Fuente, E., Mergen, C., Bour, S., Thaler, J.P., Seeley, R.J., et al. (2014). Hormones and diet, but not body weight, control hypothalamic microglial activity. Glia *62*, 17–25.

Gautier, E.L., Shay, T., Miller, J., Greter, M., Jakubzick, C., Ivanov, S., Helft, J., Chow, A., Elpek, K.G., Gordonov, S., et al.; Immunological Genome Consortium (2012). Gene-expression profiles and transcriptional regulatory pathways that underlie the identity and diversity of mouse tissue macrophages. Nat. Immunol. *13*, 1118–1128.

Ghosn, E.E., Cassado, A.A., Govoni, G.R., Fukuhara, T., Yang, Y., Monack, D.M., Bortoluci, K.R., Almeida, S.R., Herzenberg, L.A., and Herzenberg, L.A. (2010). Two physically, functionally, and developmentally distinct peritoneal macrophage subsets. Proc. Natl. Acad. Sci. U S A *107*, 2568–2573.

Gosselin, D., Link, V.M., Romanoski, C.E., Fonseca, G.J., Eichenfield, D.Z., Spann, N.J., Stender, J.D., Chun, H.B., Garner, H., Geissmann, F., and Glass, C.K. (2014). Environment drives selection and function of enhancers controlling tissue-specific macrophage identities. Cell *159*, 1327–1340.

Henstridge, D.C., Whitham, M., and Febbraio, M.A. (2014). Chaperoning to the metabolic party: The emerging therapeutic role of heat-shock proteins in obesity and type 2 diabetes. Mol. Metab. *3*, 781–793.

Huang, X., Feng, Z., Jiang, Y., Li, J., Xiang, Q., Guo, S., Yang, C., Fei, L., Guo, G., Zheng, L., et al. (2019). VSIG4 mediates transcriptional inhibition of Nlrp3 and Il-1beta in macrophages. Sci. Adv. *5*, eaau7426.

Jablonski, K.A., Amici, S.A., Webb, L.M., Ruiz-Rosado, Jde.D., Popovich, P.G., Partida-Sanchez, S., and Guerau-de-Arellano, M. (2015). Novel markers to delineate murine M1 and M2 macrophages. PLoS ONE *10*, e0145342.

Janky, R., Verfaillie, A., Imrichová, H., Van de Sande, B., Standaert, L., Christiaens, V., Hulselmans, G., Herten, K., Naval Sanchez, M., Potier, D., et al. (2014). iRegulon: from a gene list to a gene regulatory network using large motif and track collections. PLoS Comput. Biol. *10*, e1003731.

Kolde, R. (2019). pheatmap: pretty heatmaps. R package version 1.0.12. https://cran.r-project.org/web/packages/pheatmap/index.html.

Kratz, M., Coats, B.R., Hisert, K.B., Hagman, D., Mutskov, V., Peris, E., Schoenfelt, K.Q., Kuzma, J.N., Larson, I., Billing, P.S., et al. (2014). Metabolic dysfunction drives a mechanistically distinct proinflammatory phenotype in adipose tissue macrophages. Cell Metab. *20*, 614–625.

Lackie, R.E., Maciejewski, A., Ostapchenko, V.G., Marques-Lopes, J., Choy, W.Y., Duennwald, M.L., Prado, V.F., and Prado, M.A.M. (2017). The Hsp70/Hsp90 chaperone machinery in neurodegenerative diseases. Front. Neurosci. *11*, 254.

Langfelder, P., and Horvath, S. (2008). WGCNA: an R package for weighted correlation network analysis. BMC Bioinformatics *9*, 559.

Langfelder, P., and Zhang, B. (2016). dynamicTreeCut: methods for detection of clusters in hierarchical clustering dendrograms. R package version 1.63-1. http://cran.rproject.org/package=dynamicTreeCut.

Lavin, Y., Winter, D., Blecher-Gonen, R., David, E., Keren-Shaul, H., Merad, M., Jung, S., and Amit, I. (2014). Tissue-resident macrophage enhancer landscapes are shaped by the local microenvironment. Cell *159*, 1312–1326.

Lee, C.T., and Repasky, E.A. (2012). Opposing roles for heat and heat shock proteins in macrophage functions during inflammation: a function of cell activation state? Front. Immunol. *3*, 140.

Li, H., Handsaker, B., Wysoker, A., Fennell, T., Ruan, J., Homer, N., Marth, G., Abecasis, G., and Durbin, R.; 1000 Genome Project Data Processing Subgroup (2009). The Sequence Alignment/Map format and SAMtools. Bioinformatics *25*, 2078–2079.

Liao, Y., Smyth, G.K., and Shi, W. (2014). featureCounts: an efficient general purpose program for assigning sequence reads to genomic features. Bioinformatics *30*, 923–930.

Libby, P. (2012). Inflammation in atherosclerosis. Arterioscler. Thromb. Vasc. Biol. *32*, 2045–2051.

Literáti-Nagy, Z., Tory, K., Literáti-Nagy, B., Kolonics, A., Török, Z., Gombos, I., Balogh, G., Vígh, L., Jr., Horváth, I., Mandl, J., et al. (2012). The HSP co-inducer BGP-15 can prevent the metabolic side effects of the atypical antipsychotics. Cell Stress Chaperones *17*, 517–521.

Liu, T., Zhang, L., Joo, D., and Sun, S.C. (2017). NF-κB signaling in inflammation. Signal Transduct. Target. Ther. *2*, 17023.

Love, M.I., Huber, W., and Anders, S. (2014). Moderated estimation of fold change and dispersion for RNA-seq data with DESeq2. Genome Biol. *15*, 550.

Lumeng, C.N., Bodzin, J.L., and Saltiel, A.R. (2007). Obesity induces a phenotypic switch in adipose tissue macrophage polarization. J. Clin. Invest. *117*, 175–184.

Maedler, K., Sergeev, P., Ris, F., Oberholzer, J., Joller-Jemelka, H.I., Spinas, G.A., Kaiser, N., Halban, P.A., and Donath, M.Y. (2002). Glucose-induced beta cell production of IL-1beta contributes to glucotoxicity in human pancreatic islets. J. Clin. Invest. *110*, 851–860.

Malandrino, M.I., Fucho, R., Weber, M., Calderon-Dominguez, M., Mir, J.F., Valcarcel, L., Escoté, X., Gómez-Serrano, M., Peral, B., Salvadó, L., et al. (2015). Enhanced fatty acid oxidation in adipocytes and macrophages reduces lipid-induced triglyceride accumulation and inflammation. Am. J. Physiol. Endocrinol. Metab. *308*, E756–E769.

Martinez, F.O., and Gordon, S. (2014). The M1 and M2 paradigm of macrophage activation: time for reassessment. F1000Prime Rep. *6*, 13.

Merico, D., Isserlin, R., Stueker, O., Emili, A., and Bader, G.D. (2010). Enrichment Map: a network-based method for gene-set enrichment visualization and interpretation. PLoS ONE *5*, e13984.

Moore, K.J., Sheedy, F.J., and Fisher, E.A. (2013). Macrophages in atherosclerosis: a dynamic balance. Nat. Rev. Immunol. *13*, 709–721.

Murray, P.J., Allen, J.E., Biswas, S.K., Fisher, E.A., Gilroy, D.W., Goerdt, S., Gordon, S., Hamilton, J.A., Ivashkiv, L.B., Lawrence, T., et al. (2014). Macrophage activation and polarization: nomenclature and experimental guidelines. Immunity *41*, 14–20.

O'Neill, L.A., Kishton, R.J., and Rathmell, J. (2016). A guide to immunometabolism for immunologists. Nat. Rev. Immunol. *16*, 553–565.

Nackiewicz, M.D., Speck, M., Chow, S., Pospisilik, J.A., Verchere, B., and Ehses, J. (2020). Islet macrophages are the primary islet source of IGF-1 and improve glucose homeostasis following pancreatic beta-cell death. iScience. https://doi.org/10.1016/j.isci.2019.100775.

Oh, J., Riek, A.E., Weng, S., Petty, M., Kim, D., Colonna, M., Cella, M., and Bernal-Mizrachi, C. (2012). Endoplasmic reticulum stress controls M2 macrophage differentiation and foam cell formation. J. Biol. Chem. *287*, 11629–11641.

Okabe, Y., and Medzhitov, R. (2014). Tissue-specific signals control reversible program of localization and functional polarization of macrophages. Cell *157*, 832–844.

Okonechnikov, K., Conesa, A., and García-Alcalde, F. (2016). Qualimap 2: advanced multi-sample quality control for high-throughput sequencing data. Bioinformatics *32*, 292–294.

Pal, D., Dasgupta, S., Kundu, R., Maitra, S., Das, G., Mukhopadhyay, S., Ray, S., Majumdar, S.S., and Bhattacharya, S. (2012). Fetuin-A acts as an endogenous ligand of TLR4 to promote lipid-induced insulin resistance. Nat. Med. *18*, 1279–1285.

Picelli, S., Faridani, O.R., Björklund, A.K., Winberg, G., Sagasser, S., and Sandberg, R. (2014). Full-length RNA-seq from single cells using Smart-seq2. Nat. Protoc. *9*, 171–181.

Rath, M., Müller, I., Kropf, P., Closs, E.I., and Munder, M. (2014). Metabolism via arginase or nitric oxide synthase: two competing arginine pathways in macrophages. Front. Immunol. *5*, 532.

Richardson, S.J., Willcox, A., Bone, A.J., Foulis, A.K., and Morgan, N.G. (2009). Islet-associated macrophages in type 2 diabetes. Diabetologia *52*, 1686–1688.

Sanyal, R., Polyak, M.J., Zuccolo, J., Puri, M., Deng, L., Roberts, L., Zuba, A., Storek, J., Luider, J.M., Sundberg, E.M., et al. (2017). MS4A4A: a novel cell surface marker for M2 macrophages and plasma cells. Immunol. Cell Biol. *95*, 611–619.

Schopf, F.H., Biebl, M.M., and Buchner, J. (2017). The HSP90 chaperone machinery. Nat. Rev. Mol. Cell Biol. *18*, 345–360.

Shannon, P., Markiel, A., Ozier, O., Baliga, N.S., Wang, J.T., Ramage, D., Amin, N., Schwikowski, B., and Ideker, T. (2003). Cytoscape: a software environment for integrated models of biomolecular interaction networks. Genome Res. *13*, 2498–2504.

Sheedy, F.J., Grebe, A., Rayner, K.J., Kalantari, P., Ramkhelawon, B., Carpenter, S.B., Becker, C.E., Ediriweera, H.N., Mullick, A.E., Golenbock, D.T., et al. (2013). CD36 coordinates NLRP3 inflammasome activation by facilitating intracellular nucleation of soluble ligands into particulate ligands in sterile inflammation. Nat. Immunol. *14*, 812–820.

Subramanian, A., Tamayo, P., Mootha, V.K., Mukherjee, S., Ebert, B.L., Gillette, M.A., Paulovich, A., Pomeroy, S.L., Golub, T.R., Lander, E.S., and Mesirov, J.P. (2005). Gene set enrichment analysis: a knowledge-based approach for interpreting genome-wide expression profiles. Proc. Natl. Acad. Sci. U S A *102*, 15545–15550.

Swinton, J. (2019). Vennerable: Venn and Euler area-proportional diagrams. R package version 3.1.0.9000. https://github.com/js229/Vennerable.

Valdearcos, M., Robblee, M.M., Benjamin, D.I., Nomura, D.K., Xu, A.W., and Koliwad, S.K. (2014). Microglia dictate the impact of saturated fat consumption on hypothalamic inflammation and neuronal function. Cell Rep. *9*, 2124–2138.

Varesio, L., Radzioch, D., Bottazzi, B., and Gusella, G.L. (1992). Ribosomal RNA metabolism in macrophages. Curr. Top. Microbiol. Immunol. *181*, 209–237.

Veremeyko, T., Yung, A.W.Y., Anthony, D.C., Strekalova, T., and Ponomarev, E.D. (2018). Early growth response gene-2 is essential for M1 and M2 macrophage activation and plasticity by modulation of the transcription factor CEBPβ. Front. Immunol. *9*, 2515.

Weisberg, S.P., McCann, D., Desai, M., Rosenbaum, M., Leibel, R.L., and Ferrante, A.W., Jr. (2003). Obesity is associated with macrophage accumulation in adipose tissue. J. Clin. Invest. *112*, 1796–1808.

Wernstedt Asterholm, I., Tao, C., Morley, T.S., Wang, Q.A., Delgado-Lopez, F., Wang, Z.V., and Scherer, P.E. (2014). Adipocyte inflammation is essential for healthy adipose tissue expansion and remodeling. Cell Metab. *20*, 103–118.

Wickham, H. (2016). ggplot2: Elegant Graphics for Data Analysis (Springer-Verlag).

Xie, Y., Chen, C., Stevenson, M.A., Auron, P.E., and Calderwood, S.K. (2002). Heat shock factor 1 represses transcription of the IL-1beta gene through physical interaction with the nuclear factor of interleukin 6. J. Biol. Chem. *277*, 11802–11810.

Xu, H., Barnes, G.T., Yang, Q., Tan, G., Yang, D., Chou, C.J., Sole, J., Nichols, A., Ross, J.S., Tartaglia, L.A., and Chen, H. (2003). Chronic inflammation in fat plays a crucial role in the development of obesity-related insulin resistance. J. Clin. Invest. *112*, 1821–1830.

Xue, J., Schmidt, S.V., Sander, J., Draffehn, A., Krebs, W., Quester, I., De Nardo, D., Gohel, T.D., Emde, M., Schmidleithner, L., et al. (2014).

Transcriptome-based network analysis reveals a spectrum model of human macrophage activation. Immunity *40*, 274–288.

Ying, W., Lee, Y.S., Dong, Y., Seidman, J.S., Yang, M., Isaac, R., Seo, J.B., Yang, B.H., Wollam, J., Riopel, M., et al. (2019). Expansion of islet-resident macrophages leads to inflammation affecting β cell proliferation and function in obesity. Cell Metab. *29*, 457–474.e5.

Zhang, B., and Horvath, S. (2005). A general framework for weighted gene co-expression network analysis. Stat. Appl. Genet. Mol. Biol. *4*, Article 17.

Zhou, R., Tardivel, A., Thorens, B., Choi, I., and Tschopp, J. (2010). Thioredoxin-interacting protein links oxidative stress to inflammasome activation. Nat. Immunol. *11*, 136–140.

STAR★METHODS

KEY RESOURCES TABLE

REAGENT or RESOURCE	SOURCE	IDENTIFIER
Antibodies		
anti-mouse CD16/CD32 [clone 93]	Thermo Fisher Scientific	Cat# 14-0161-85; RRID: AB_467134
APC anti-mouse CD45 [clone 30-F11]	Thermo Fisher Scientific	Cat# 17-0451-83; RRID: AB_469392
PE anti-mouse CD11b [clone M1/70]	Thermo Fisher Scientific	Cat# 12-0112-81; RRID: AB_465546
PECy7 anti-mouse F4/80 [clone BM8]	Thermo Fisher Scientific	Cat# 25-4801-82; RRID: AB_465923
APC anti-mouse CD115 [clone AFS98]	Thermo Fisher Scientific	Cat# 17-1152-82; RRID:AB_1210789
PerCP-Cyanine5.5 anti-mouse Ly6C [clone HK1.4]	Thermo Fisher Scientific	Cat# 45-5932-82; RRID:AB_2723343
APC-Cy7 anti-mouse Ly6G [clone 1A8]	BioLegend	Cat# 127624; RRID:AB_10640819
PE-Cy7 anti-mouse CD11c [clone N418]	Thermo Fisher Scientific	Cat# 25-0114-81; RRID:AB_469589
Super Bright 600 anti-mouse CD19 [clone 1D3]	Thermo Fisher Scientific	Cat# 63-0193-82; RRID:AB_2637308
PE-Texas Red anti-mouse CD11b [clone M1/70.15]	Thermo Fisher Scientific	Cat# RM2817; RRID:AB_1464525
PerCP-Cy5.5 anti-mouse F4/80 [clone BM8]	BioLegend	Cat# 123127; RRID:AB_893496
APC-Cy7 anti-mouse F4/80 [clone BM8]	BioLegend	Cat# 123118; RRID:AB_893477
Alexa Fluor 647 anti-mouse CD206 [clone C068C2]	BioLegend	Cat# 141712; RRID:AB_10900420
PE anti-mouse iNOS [clone CXNFT]	Thermo Fisher Scientific	Cat# 12-5920-82; RRID:AB_2572642
Chemicals, Peptides, and Recombinant Proteins		
Trypsin	GIBCO	Cat# 154000-054
BPG-15	Sigma-Aldrich	Cat# B4813-5MG
LPS	InvivoGen	Cat# tlrl-smlps
Collagenase type 4	Worthington	Cat# CLS-4
ATP	InvivoGen	Cat# tlr-atp
Fixable Viability Dye eFluor 455UV	Thermo Fisher Scientific	Cat# 65-0868-18
DNA-binding dye DAPI	BioLegend	Cat# 422801
Streptozotocin	Sigma-Aldrich	Cat# S0130
0.5% Trypsin-EDTA (x10)	Thermo Fisher Scientific	Cat# 15400054
Bovine Serum Albumin (Fatty acid free – Low endotoxin)	Sigma-Aldrich	Cat# A8806
Critical Commercial Assays		
Mouse/rat insulin kit	Meso Scale Discovery	Cat# K152BZC
V-plex mouse IL-1β kit	Meso Scale Discovery	Cat# K152QPD-1
Nucleo Spin RNA II Kit	Machery Nagel	Cat# 740955.250
GoScript Reverse Transcription Mix using Random Primers	Promega	Cat# A2801
GoTaq qPCR Master Mix	Promega	Cat# A600A
Arcturus PicoPure RNA Isolation Kit	Thermo Fisher Scientific	Cat# KIT0204
RNase-Free DNase Set	QIAGEN	Cat# 79254
Quant-iT RiboGreen RNA Assay Kit	Thermo Fisher Scientific	Cat# R11490
intracellular Fixation and Permeabilization Buffer Set	Thermo Fisher Scientific	Cat# 88-8824

(*Continued on next page*)

Continued

REAGENT or RESOURCE	SOURCE	IDENTIFIER
Deposited Data		
bulk RNaseq data of mouse macrophage subsets isolated from different tissues upon acute and chronic metabolic challange	This manuscript	GEO: GSE133127
Tissue macrophage transcriptomes	Lavin et al., 2014; GEO: GSE63341	https://doi.org/10.1016/j.cell.2014.11.018
Gene signatures of macrophage responses to 29 *in-vitro* stimuli	Xue et al., 2014; Table S2	https://doi.org/10.1016/j.immuni.2014.01.006
Experimental Models: Organisms/Strains		
C57BL/6NCrl *Mus musculus*	in-house breeding (originated from Charles River Germany)	MGI:2683688; Strain Code 027; RRID:IMSR_CRL:027
Oligonucleotides		
18S FW: CTCAACACGGGAAACCTCAC	Microsynth	N/A
18S REV: CGCTCCACCAACTAAGAACG	Microsynth	N/A
B2 FW: TTCTGGTGCTTGTCTCACTGA	Microsynth	N/A
B2 REV: CAGTATGTTCGGCTTCCCATTC	Microsynth	N/A
Il1b FW: GCAACTGTTCCTGAACTCAACT	Microsynth	N/A
Il1b REV: ATCTTTTGGGGTCCGTCAACT	Microsynth	N/A
Ccl3 FW: CCATATGGAGCTGACACCCC	Microsynth	N/A
Ccl3 REV: GTCAGGAAAATGACACCTGGC	Microsynth	N/A
Cxcl1 FW: ACCGAAGTCATAGCCACACTC	Microsynth	N/A
Cxcl1 REV: CTCCGTTACTTGGGGACACC	Microsynth	N/A
Nfkbid FW: CCCACAGTCTGCATCCAAGAA	Microsynth	N/A
Nfkbid REV: ATGAGTATGGCCTGGCTCTG	Microsynth	N/A
Nfkbiz FW: GAAACCCAGCCGTCTTCTGA	Microsynth	N/A
Nfkbiz REV: CTACGCGGTTGGCCTCG	Microsynth	N/A
Tlr2 FW: AAACCTCAGACAAAGCGTCAA	Microsynth	N/A
Tlr2 REV: TTCATGGCTGCTGTGAGTCC	Microsynth	N/A
Actb FW: GGCTGTATTCCCCTCCATCG	Microsynth	N/A
Actb REV: CCAGTTGGTAACAATGCCATGT	Microsynth	N/A
Software and Algorithms		
Prism 8	Graphpad Prism	https://www.graphpad.com; RRID: SCR_002798
FlowJo 10.6.1 software	Tree Star	https://www.flowjo.com/solutions/flowjo/downloads; RRID:SCR_008520
FastQC (version 0.11.5)	http://www.bioinformatics.babraham.ac.uk/projects/fastqc/	RRID:SCR_014583
Trimmomatic (version 0.36)	https://doi.org/10.1093/bioinformatics/btu170	http://www.usadellab.org/cms/index.php?page=trimmomatic; RRID:SCR_011848
STAR (version 2.5.1a)	https://doi.org/10.1093/bioinformatics/bts635	https://github.com/alexdobin/STAR; RRID:SCR_015899
SAM tools (version 1.4)	https://doi.org/10.1093/bioinformatics/btp352	https://www-stat.stanford.edu/~tibs/SAM/ ; RRID:SCR_010951
Qualimap (version 2.2.1)	https://academic.oup.com/bioinformatics/article/32/2/292/1744356	http://qualimap.bioinfo.cipf.es/; RRID:SCR_001209
R subread package (version v1.30.4)	https://doi.org/10.1093/bioinformatics/btt656	http://subread.sourceforge.net/; RRID:SCR_009803
R (version 3.4.1)	www.r-project.org	N/A

(*Continued on next page*)

Continued

REAGENT or RESOURCE	SOURCE	IDENTIFIER
DESeq2 (version 1.18.1)	https://doi.org/10.1186/s13059-014-0550-8	http://bioconductor.org/packages/release/bioc/html/DESeq2.html; RRID:SCR_000154
ggplot2 (version 3.1.0)	https://www.springer.com/de/book/9783319242750	https://cran.r-project.org/web/packages/ggplot2/index.html; RRID:SCR_014601
pheatmap (version 1.0.12) (Kolde, 2019)	https://github.com/raivokolde/pheatmap, https://cran.r-project.org/web/packages/pheatmap/pheatmap.pdf	https://www.rdocumentation.org/packages/pheatmap/versions/0.2/topics/pheatmap; RRID:SCR_016418
EGSEA (version 1.10.1)	https://doi.org/10.12688/f1000research.12544.1	http://bioconductor.org/packages/release/bioc/html/EGSEA.html; RRID:SCR_015036
EnrichmentMap (version 3.0.0)	https://doi.org/10.1371/journal.pone.0013984	http://baderlab.org/Software/EnrichmentMap; RRID:SCR_016052
Cytoscape software (version 3.7.1)	https://doi.org/10.1101/gr.1239303	https://cytoscape.org; RRID:SCR_003032
iRegulon (version 1.3)	https://dx.plos.org/10.1371/journal.pcbi.1003731	http://iregulon.aertslab.org/download.html
Weighted Gene Correlation Network Analysis (WGCNA) R package (version 1.66)	(Langfelder and Horvath, 2008).	https://horvath.genetics.ucla.edu/html/CoexpressionNetwork/Rpackages/WGCNA/; RRID:SCR_003302
Dynamic tree cut (dynamicTreeCut R-package, version 1.63)	https://cran.r-project.org/src/contrib/dynamicTreeCut_1.63-1.tar.gz	https://cran.r-project.org/web/packages/dynamicTreeCut/dynamicTreeCut.pdf
biomaRt R package (version 2.38.0)	https://doi.org/10.1038/nprot.2009.97	http://bioconductor.org/packages/release/bioc/html/biomaRt.html
GSEA software (version 3.0)	http://software.broadinstitute.org/gsea/index.jsp	https://www.broadinstitute.org/gsea/; RRID:SCR_003199
Vennerable (version 3.1.0.9)	https://github.com/js229/Vennerable	https://github.com/js229/Vennerable
Other		
high-fat diet (58% fat, 26% carbohydrates and 16% protein)	Research Diets	Cat# D12331
high-fat diet	ssniff Spezialitäten, Soest, Germany	Cat# EF D12492 (I) mod. 60 kJ% fat [Lard]

LEAD CONTACT AND MATERIALS AVAILABILITY

Further information and requests for resources and reagents should be directed to and will be fulfilled by the Lead Contact, Sophia Julia Wiedemann (sophia.j.wiedemann@gmail.com). This study did not generate new unique reagents.

EXPERIMENTAL MODEL AND SUBJECT DETAILS

Experimental mice were obtained from our in-house breeding (littermate C57BL/6N). All mice were male, unless otherwise specified. The age of the mice used for individual experiments is specified below. Littermates of the same sex were randomly assigned to experimental groups unless otherwise specified. All animal experiments were approved by the Swiss Authorities and conducted according to local Institutional Guidelines and the Swiss Veterinary Law. Wherever possible, each cage included mice receiving all treatments in order to avoid cage-dependent effects.

METHOD DETAILS

Animal husbandry

All animals were housed in a temperature-controlled room with a 12 h light–12 h dark cycle and free access to food and water unless otherwise indicated. Fasting and refeeding experiments were performed at 8 weeks of age and as previously described in Dror et al. (2017) using weight-matched littermate male mice: ''mice were fasted overnight for 12 hours meaning they were provided free access to water but not to food. Refed mice were then allowed access to the food they were accustomed to for a period of 2h, while fasted mice were kept fasted for an additional 2 hours. To avoid potential confounding effects due to circadian-cycle-mediated fluctuations in circulating IL-1β concentrations, all experiments were performed at the same time of the day (between 8 a.m. and 10 a.m.).''

For HFD-STZ experiments, initially weight-matched 9-week old littermate male mice were either kept on normal CHOW (= ND condition) or fed a high-fat diet (D12331, Research Diets; 58% fat, 26% carbohydrates and 16% protein, = HFD condition) for 8 more weeks total. During the fourth week of high-fat diet feeding, mice were subjected to an intraperitoneal injection of either 130 mg/kg Streptozotocin (Sigma, dissolved in citrate buffer (pH 4.5), = HFD-STZ condition) or control solution (0.9% saline).

Primary cell isolation

Monocytes, peritoneal macrophages, Kupffer cells, adipose-tissue macrophages and colonic macrophages were isolated as described in Dror et al. (2017).

Briefly, and taken/adapted from Dror et al.: following euthanasia in a CO_2 chamber, ''the mouse heart was punctured, and the collected blood was incubated briefly with red-blood-cell lysis buffer (154 mM NH_4Cl, 10 mM $KHCO_3$ and 0.1 mM EDTA) to obtain circulating blood leukocytes. To isolate peritoneal macrophages, the peritoneum was infused with FACS buffer (PBS with 0.5% BSA and 5 mM EDTA) and the lavage was filtered through 70-μm cell strainer (#431751, Corning). Kupffer cells were isolated from the liver perfused with 4 ml collagenase (1.4 gr/l; collagenase type 4; Worthington) through the ductal vein followed by a 30-min incubation step at 37°C and two centrifugation steps: 50 × *g* for 3 min at 4°C, collection of the upper phase and 350 × *g* for 5 min at 4°C. Intestinal macrophages were isolated after removal of the intestinal payer patches, cut in pieces and washed twice (20 min shaking in PBS with 5 mM EDTA), followed by 30 min of incubation in collagenase type 4 (1.4 gr/l; Worthington) at 37°C. Cells from the epididymal fat pads were isolated after shaking with collagenase type 4 (1.4 gr/l; Worthington) for 30 min at 37°C. Spleens were pushed through a 70-μm cell strainer (#431751, Corning) and red blood cells were lysed using lysis buffer (154 mM NH_4CL, 10 mM $KHCO_3$ and 0.1 mM EDTA).''

Islet macrophages were isolated as described in Dalmas et al., 2017. Briefly, and taken from Dalmas et al. (2017): ''To isolate mouse islets, pancreata were perfused through the common bile duct with a HBSS collagenase solution (1.4 g/L; collagenase type 4 Worthington) and digested in the same solution in a 37°C water bath for 28 min. After shaking for 15 seconds, pancreata were washed three times with HBSS supplemented with 0.5% bovine serum albumin (BSA) and filtrated through 500 μm and 70 μm cell strainers (Corning). Islets were retained on the 70 μm cell strainer while the cell mixture passing through the 70 μm cell strainer represented the exocrine stoma. Islets from the same condition were handpicked and pooled into a Petri dish with RPMI-1640 (GIBCO) containing 11.1 mM glucose, 100 units/ml penicillin, 100 mg/ml streptomycin, 2 mM Glutamax, 50 mg/ml gentamycin, 10 mg/ml Fungison and 10% FCS (Invitrogen). To obtain single cells, islets were gently dispersed with a 0.0125% trypsin-EDTA (GIBCO) solution for 2 min in a 37°C water bath, washed with cold FACS buffer (PBS with 0.5% BSA and 5 mM EDTA), centrifuged at 300 x g, 4°C for 5 min and resuspended in FACS buffer.''

Microglia were isolated from mice treated as described above following euthanasia in a CO_2 chamber. Briefly, mice were initially perfused with an ice-cold 0.9% saline solution. Whole brains were then excised from the skull and mechanically dissociated in FACS buffer (PBS with 0.5% BSA and 5 mM EDTA) using a Dounce-homogenizer (#D9938-1SET, Merck). Cells were then passed through a 70-μm cell strainer (#431751, Corning), washed with FACS buffer (PBS with 0.5% BSA and 5 mM EDTA) and dissolved in a 37% isotonic Percoll solution (#17-0891-01, GE Healthcare). 37% Percoll was then layered on top of a 70% isotonic Percoll solution and centrifuged for 30 minutes at 750 × *g* using minimal brake. The microglia-containing interphase was subsequently collected and filtered through a 70-μm cell strainer, washed and again resuspended in FACS buffer (PBS with 0.5% BSA and 5 mM EDTA).

Cell culture

For the culture of peritoneal macrophages, cells were allowed to adhere for at least 3 h in 60 × 15 mm circular cell culture dishes (#82.1194.500, Sarstedt). Then non-adherent cells were washed away vigorously, and naive macrophages were used for cytokine-release assays. Briefly, naive peritoneal macrophages were seeded into standard 96-well plates (#92097, TPP) at a density of 50'000 cells/well following trypsinization (#154000-054, GIBCO). Cells were pre-incubated either at 37°C (control condition) or 41°C (heat condition) ± BPG-15 (50mM, #B4813-5MG, Sigma) for 30 minutes. Following pre-incubation, cells were primed for 3h with 100 ng/ml LPS (#tlrl-smlps, InvivoGen). Then, cytokine release was induced by a further 30 min incubation step with ATP (5 mM; #tlr-atp, InvivoGen). Supernatants were subsequently collected and centrifuged (at 4°C, 450 × *g* for 5 min) and then stored at −80°C. Remaining cells were harvested for flow cytometry and assessed for viability using the DNA-binding dye DAPI (4',6-Diamidino-2-Phenylindole, Dilactate; #422801, BioLegend).

Flow cytometry

For cell sorting

Cells were incubated with an Fc blocking antibody (anti-mouse CD16/CD32 clone 93, #14-0161-85, eBioscience) for 15 minutes at room temperature, and subsequently labeled with the following antibodies for 30 min at 4°C in the dark: APC anti-mouse CD45 [clone 30-F11] (#17-0451-83, eBioscience), PE anti-mouse CD11b [clone M1/70] (#12-0112-81, eBioscience) and PECy7 anti-mouse F4/80 [clone BM8] (#25-4801-82, eBioscience). In case of monocytes, the following antibodies were used: APC anti-mouse CD115 [clone AFS98] (#17-1152-82, eBioscience), PerCP-Cyanine5.5 anti-mouse Ly6C [clone HK1.4] (#45-5932-82, eBioscience) and APC-Cy7 anti-mouse Ly6G [clone 1A8] (#127624, BioLegend). Appropriately stained cells were then washed twice with FACS buffer (PBS with 0.5% BSA and 5 mM EDTA). Viability staining was done using the DNA-binding dye DAPI (#422801, BioLegend). Cells were then further enriched into tissue-resident macrophage populations by fluorescence-activated cell sorting (FACS) on a BD FACS-Aria

III. Monocytes were defined as live (DAPI-) single CD115+ Ly6G- Ly6C+. Adipose tissue macrophages, Kupffer cells, peritoneal macrophages, intestinal macrophages and islet macrophages were defined as live single CD45+ CD11b+ F4/80+. Microglia were defined as live single CD11b+ CD45^{int}. For a representative example of the gating strategy see Figure S1. With regards to cell number, for the refeeding experiment, 400 cells of each macrophage subtype were sorted per sample. For the HFD-STZ experiment, 400 islet macrophages, 5000 microglia and 100'000 peritoneal macrophages were sorted per sample.

For the analysis of LPM and SPM peritoneal macrophage subsets

Peritoneal cells, isolated as described above and in Dror et al. (2017) from 16 week old, 8 weeks HFD-fed (EF D12492 (I) mod. 60 kJ% fat [Lard]; ssniff Spezialitäten, Soest, Germany) or CHOW-fed littermate control mice, were incubated with an Fc blocking antibody (anti-mouse CD16/CD32 clone 93, #14-0161-85, eBioscience) for 15 minutes at room temperature, and subsequently labeled with the following antibodies for 30 min at 4°C in the dark: PE-Cy7 anti-mouse CD11c [clone N418] (#25-0114-81, eBioscience), Super Bright 600 anti-mouse CD19 [clone 1D3] (#63-0193-82, invitrogen), PE-Texas Red anti-mouse CD11b [clone M1/70.15] (#RM2817, eBioscience), PerCP-Cy5.5 anti-mouse F4/80 [clone BM8] (#123127, BioLegend) (or alternatively APC-Cy7 anti-mouse F4/80 [clone BM8] (#123118, BioLegend)) and Alexa Fluor® 647 anti-mouse CD206 [clone C068C2] (#141712, BioLegend). Viability staining was done using the Fixable Viability Dye eFluor 455UV (#65-0868-18, eBioscience) according to the manufacturer's instructions. Appropriately stained cells were then washed once with FACS buffer (PBS with 0.5% BSA and 5 mM EDTA) and further prepared for intracellular staining using the intracellular Fixation and Permeabilization Buffer Set (#88-8824, eBioscience) and protocol. Intracellular staining was done using the following antibody: PE anti-mouse iNOS [clone CXNFT] (#12-5920-82, Invitrogen). Cells were analyzed on a BC CytoFLEX. Small peritoneal macrophages (SPM) were defined as live single CD19- CD11c- F4/80^{low} CD11b^{low}. Large peritoneal macrophages (LPM) were defined as live single CD19- CD11c- F4/80^{high} CD11b^{high}. Gating was performed uniquely with reference to fluorescence minus one controls (FMOs). For a representative example of the gating strategy see Figure S7.

RNA extraction for validation and qPCR

Total RNA was extracted using the Nucleo Spin RNA II Kit (Machery Nagel). RNA concentrations were normalized, and cDNA was prepared with the GoScript Reverse Transcription Mix using Random Primers (#A2801 GoScript) according to the manufacturer's instructions. RNA expression was determined using SYBR Green assays with GoTaq qPCR Master Mix (#A600A Promega) and the ViiA 7 Real-Time PCR System (ThermoFisher Scientific). Primers for SYBR Green-based qPCR are listed in the Key Resource Table. Data were normalized to the geometrical mean of *Actb*, *18S* and *B2* values and quantified using the comparative $2^{-\Delta\Delta CT}$method.

Assays for protein measurements

Insulin concentrations were determined using mouse/rat insulin kits (#K152BZC-1 Mesoscale Discovery) according to the manufacturer's instructions. Mouse IL-1β concentrations in cell supernatants were analyzed using the V-plex mouse IL-1β kit from Mesoscale Discovery (#K152QPD-1, Alternate Protocol 1, Extended Incubation).

RNA extraction for RNA-Seq

For RNA-Seq experiments, total RNA was isolated from macrophages and monocytes using an adapted protocol based on the Arcturus PicoPure RNA Isolation Kit method (Applied Biosystems, Thermo Fisher Scientific, USA). Cells were directly sorted into 50 μL extraction buffer supplied in the kit and incubated for 30 min at 42°C shaking. Samples were centrifuged at 3,000 x g for 5 min at 4°C and supernatants were stored at −80°C until further processing. After thawing, equal volumes of 70% (v/v) ethanol were added to the RNA samples and samples were loaded onto pre-conditioned purification columns. After a washing step, DNase on-column treatment was performed with the RNase-Free DNase Set (QIAGEN, Germany) to remove residual genomic DNA. For this purpose, a mix of 5 μL DNase I stock solution and 35 μL RDD buffer was added to the purification column membrane and incubated for 15 min at room temperature. After several washing steps, RNA was eluted from the column in 15 μl elution buffer. In contrast to this protocol, total RNA from peritoneal macrophages in the ND-HFD-STZ experiment was extracted using the NucleoSpin RNA isolation kit (Macherey-Nagel, Germany) according to the manufacturer's instructions.

Integrity of isolated total RNA was assessed on a 2100 Bioanalyzer System (Agilent Technologies, USA) and RNA concentration was measured with the Quant-iT RiboGreen RNA Assay Kit (Thermo Fisher Scientific, USA).

Sample preparation and RNA sequencing

Purification of poly(A)-containing mRNA, mRNA fragmentation and cDNA library preparation for RNA-Seq were performed using a standard Smart-seq2 protocol (Picelli et al., 2014). cDNA libraries from macrophages and monocytes were sequenced as single-end reads with 125 cycles on a HiSeq2500 sequencer (Illumina, USA) at the Genomics Facility Basel.

Processing of RNA-Seq data

Between 20 and 30 million reads were sequenced per sample. The quality of raw reads was assessed with FastQC (version 0.11.5, http://www.bioinformatics.babraham.ac.uk/projects/fastqc). SmartSeq2 and Illumina adapters and low quality sequences were trimmed with Trimmomatic (version 0.36) (Bolger et al., 2014). Trimmed sequences were aligned to the mouse reference genome

build GRCm38 (mm10) using STAR (version 2.5.1a) (Dobin et al., 2013) allowing for maximum 5% mismatching bases per read. Generated alignment (BAM) files were indexed with SAM tools (version 1.4) (Li et al., 2009). Quality of the alignment was evaluated with Qualimap (version 2.2.1) (Okonechnikov et al., 2016). Reads per gene were counted with the featureCounts function of the Rsubread package (version v1.30.4) (Liao et al., 2014) using gencode version M13 gene annotation file (https://www.gencodegenes.org). Reads mapping to multiple sequences were not counted. Raw sequences corresponding to our study as well as count tables of fasting-refeeding and HFD experiments can be retrieved at the NCBI GEO database under accession number GEO: GSE133127

QUANTIFICATION AND STATISTICAL ANALYSIS

General Information

The number of replicates analyzed was: In the transcriptomic analysis: ATM FA: 7, RE: 10, monocytes FA: 8, RE: 9, microglia FA: 8, RE: 8, colonic macrophages FA: 8, RE: 10, islet macrophages FA: 6, RE: 8, Kupffer cells FA: 6, RE: 7, peritoneal macrophages FA: 8, RE: 8, islet macrophages HFD: 4, HFD-STZ: 3, ND: 4, peritoneal macrophages HFD: 4, HFD-STZ: 5, ND: 5, microglia HFD: 4, HFD-STZ: 4, ND: 4. Statistical parameters (reported measures of dispersion and summary measures) can be found in the figure legends. Statistical assumptions for one-way ANOVA were tested beforehand (normality, homoscedasticity) and found to be met.

Differential expression analysis

Genes with low counts were filtered out using following criteria: after normalization of counts to the library size, only genes with more than 10 counts in (n-1) of n replicates in at least one experimental group (FA or RE for refeeding experiment or ND, HFD or HFD-STZ for high-fat diet experiment) were retained. Differential expression analysis was performed in R (version 3.4.1, www.r-project.org) using DESeq2 (version 1.18.1) and Wald test (Love et al., 2014). Batch information was included in the model and used as a blocking factor. Batch information can be found in the metadata table (GEO: GSE133127). P values were adjusted to obtain the false discovery rate (FDR) using the Benjamini & Hochberg method (Benjamini and Hochberg, 1995). Reported log2fold changes were obtained by shrinkage with lfcShrink default DESeq2 function. For each comparison, two tests were performed: one using a model that included all data and a contrast for a given comparison and another one with a model that included only the samples that were compared. This accounted for different dispersion of macrophage subtype-specific genes and similar dispersion of commonly expressed genes. Genes passing the adjusted p value threshold of 0.05 in either test were called differentially expressed and used in further analysis.

For differential expression analysis of all RE versus of FA samples in Figure 4, genes with low counts were filtered out using the following criteria: after normalization of counts to the library size, only genes with more than 10 counts in more than 80% of the samples were retained. Differential expression analysis was performed with the DESeq2 R package as described above and the macrophage subtype was used in the design formula as a blocking factor.

The R packages ggplot2 (version 3.1.0) (Wickham, 2016), pheatmap (version 1.0.12) (Kolde, 2019) and Vennerable (version 3.1.0.9) (Swinton, 2019) were used for data visualization.

Principal component analysis (PCA)

For PCA in Figures 1C, 1D, and 5B, raw counts were normalized to library size and transformed using the variance stabilizing transformation (vst) function of DESeq2. Only genes with more than 10 counts in more than 80% of the samples were analyzed. The plotPCA function from the DESeq2 package was used to plot PCA of top 500 variable genes. For Figure 1D, published raw RNA-Seq data from microglia, Kupffer cells, colonic and peritoneal macrophages and monocytes from Lavin et al. (2014) were processed exactly as our data (two replicates per macrophage subtype). Counts of the samples from the study by Lavin et al. (2014) and our FA samples from corresponding macrophage subtypes were together normalized to the library size and transformed using the vst function. Only genes with more than 10 counts in more than 80% of the samples were analyzed. PCA for top 500 variable genes was plotted.

Gene set and TF motive enrichment

GO term and pathway over-representation analysis were performed used EGSEA (version 1.10.1) (Alhamdoosh et al., 2017) R package. For pathways analyses, Kegg (https://www.kegg.jp) and MSigDB (http://software.broadinstitute.org/gsea/msigdb/index.jsp) canonical pathway databases were used. Over-representation analysis by hypergeometric test (implemented in the EGSEA package) was used for p value calculation with adjustment of p values using the Benjamini & Hochberg method. All expressed genes as retained after filtering in a given analyzed macrophage subtype or subtypes were used as a background dataset. For Figure 1E, over-represented GO terms among upregulated genes in each macrophage subtype were sorted based on the adjusted p values. Top 25 GO terms in each subtype passing the 0.05 adjusted p value threshold were visualized using Enrichment map (version 3.0.0) (Merico et al., 2010) app in Cytoscape software (version 3.7.1) (Shannon et al., 2003). For Figures 2B and 4C, pathways passing the 0.05 adjusted p-vale threshold were sorted based on the number of DE genes contributing to the over-representation. Top five (Figure 4C) or top ten (Figure 2B) pathways are displayed. TF motive enrichment analysis was performed using iRegulon (version 1.3) (Janky et al., 2014) and visualization of putative gene regulatory networks was performed in Cytoscape (version 3.7.1) (Shannon et al., 2003).

Clustering of genes with correlated expression pattern

To obtain clusters of genes with correlated expression across ND, HFD and HFD-STZ conditions for each analyzed macrophage subtype, we used the Weighted Gene Correlation Network Analysis (WGCNA) R package (version 1.66) (Langfelder and Horvath, 2008). DE genes from HFD versus ND and HFD-STZ versus ND comparison were combined and their counts were transformed using variance stabilizing transformation (vst) DESeq2 function. These were used to construct a signed co-expression network. A soft-threshold power used to create the pairwise distance matrix was defined as the lowest power for which the scale-free topology fit index reaches 0.80. Dynamic tree cut (dynamicTreeCut R-package, version 1.63) (Langfelder and Zhang, 2016) was used to define modules of co-expressed genes. For visualization in Figure 5, mean values of biological replicates in each condition were calculated for each gene and a relative level (mean subtraction) was displayed. Overlaps between the modules were evaluated using Fisher's exact test. GO term analysis was performed by EGSEA R package as described above and representative significantly over-represented terms from each module are displayed in Figure 5H.

Signature enrichment analysis

To determine which stimuli signatures reported by Xue et al. (2014) are enriched in our data, we followed the methodology described in Xue et al. (2014). Briefly, mouse genes detected in a given macrophage subtype (peritoneal, islet and microglia were analyzed) were translated into their human homologs using Ensembl database queried with biomaRt R package (version 2.38.0) (Durinck et al., 2009) and sorted based on the differential expression results (-log10 of the adjusted p value multiplied by the sign of the log2fold change). Sorted lists were used to analyze enrichment of 49 signatures provided by Xue et al. (2014) in Table S2 using GSEA software (version 3.0) (Subramanian et al., 2005) in a pre-ranked, weighted mode.

Analyses of functional and validation studies

For the details of these analyses see figure legends: Figure 3D and Figures S4, S5, S6A–S6C, and S7.

DATA AND CODE AVAILABILITY

All sequencing data newly generated by this study have been deposited at the NCBI's public functional genomics data repository Gene Expression Omnibus (The accession number for the dataset reported in this paper is: GEO: GSE133127, processed data are available on Series record, raw data are available in SRA) and will be made available upon publication. The publicly available dataset used in the paper (Lavin et al., 2014) can be found at GEO: GSE63341. All major software and code used to analyze this dataset are referenced above.